



“Slow walk” mimetic tensile loading maintains human meniscus tissue resident progenitor cells homeostasis in photocrosslinked gelatin hydrogel

Jing Sun^{a,b,1}, Yau Tsz Chan^{a,b}, Ki Wai Kevin Ho^c, Li Zhang^d, Liming Bian^e, Rocky S. Tuan^{a,b,f,**}, Yangzi Jiang^{a,b,f,*}

^a Institute for Tissue Engineering and Regenerative Medicine, School of Biomedical Sciences, Faculty of Medicine, The Chinese University of Hong Kong, Shatin, Hong Kong Special Administrative Region of China

^b School of Biomedical Sciences, Faculty of Medicine, The Chinese University of Hong Kong, Shatin, Hong Kong Special Administrative Region of China

^c Department of Orthopaedics & Traumatology, Faculty of Medicine, The Chinese University of Hong Kong, And Prince of Wales Hospital, Shatin, Hong Kong Special Administrative Region of China

^d Department of Mechanical and Automation Engineering, Faculty of Engineering, The Chinese University of Hong Kong, Shatin, Hong Kong Special Administrative Region of China

^e Department of Biomedical Engineering, Faculty of Engineering, The Chinese University of Hong Kong, Shatin, Hong Kong Special Administrative Region of China

^f Center for Neuromusculoskeletal Restorative Medicine, Hong Kong Special Administrative Region of China

ARTICLE INFO

Keywords:

Human meniscus progenitor cells
3D cell-based constructs
Biomimetic cyclic loading
GelMA hydrogel
Extracellular matrix

ABSTRACT

Meniscus, the cushion in knee joint, is a load-bearing tissue that transfers mechanical forces to extracellular matrix (ECM) and tissue resident cells. The mechanoreponse of human tissue resident stem/progenitor cells in meniscus (hMeSPCs) is significant to tissue homeostasis and regeneration but is not well understood. This study reports that a mild cyclic tensile loading regimen of ~1800 loads/day on hMeSPCs seeded in 3-dimensional (3D) photocrosslinked gelatin methacryloyl (GelMA) hydrogel is critical in maintaining cellular homeostasis. Experimentally, a “slow walk” biomimetic cyclic loading regimen (10% tensile strain, 0.5 Hz, 1 h/day, up to 15 days) is applied to hMeSPCs encapsulated in GelMA hydrogel with a magnetic force-controlled loading actuator. The loading significantly increases cell differentiation and fibrocartilage-like ECM deposition without affecting cell viability. Transcriptomic analysis reveals 332 mechanoreponsive genes, clustered into cell senescence, mechanical sensitivity, and ECM dynamics, associated with interleukins, integrins, and collagens/matrix metalloproteinase pathways. The cell-GelMA constructs show active ECM remodeling, traced using a green fluorescence tagged (GFT)-GelMA hydrogel. Loading enhances nascent pericellular matrix production by the encapsulated hMeSPCs, which gradually compensates for the hydrogel loss in the cultures. These findings demonstrate the strong tissue-forming ability of hMeSPCs, and the importance of mechanical factors in maintaining meniscus homeostasis.

Abbreviations: BMSCs, Bone marrow derived mesenchymal stem cells; Col I, Collagen type I; Col II, Collagen type II; CFUs, Colony forming units; DS, Degree of substitution; ECM, Extracellular matrix; GelMA, Gelatin methacryloyl; GAGs, Glycosaminoglycans; GFT-GelMA, Green fluorescence-tagged GelMA; hMeSPCs, Human meniscus stem/progenitor cells; MeHA, Methacrylated hyaluronic acid; PCM, Pericellular matrix; PI, Propidium iodide; PPI, Protein-protein interaction; 3D, Three-dimensional.

Peer review under responsibility of KeAi Communications Co., Ltd.

* Corresponding author. Institute for Tissue Engineering and Regenerative Medicine, School of Biomedical Sciences, Faculty of Medicine, The Chinese University of Hong Kong, Shatin, Hong Kong Special Administrative Region of China.

** Corresponding author. Institute for Tissue Engineering and Regenerative Medicine, School of Biomedical Sciences, Faculty of Medicine, The Chinese University of Hong Kong, Shatin, Hong Kong Special Administrative Region of China.

E-mail addresses: tuanr@cuhk.edu.hk (R.S. Tuan), yangzjiang21@cuhk.edu.hk (Y. Jiang).

¹ These authors contributed equally.

<https://doi.org/10.1016/j.bioactmat.2023.01.025>

Received 1 November 2022; Received in revised form 14 January 2023; Accepted 31 January 2023

2452-199X/© 2023 The Authors. Publishing services by Elsevier B.V. on behalf of KeAi Communications Co. Ltd. This is an open access article under the CC BY-NC-ND license (<http://creativecommons.org/licenses/by-nc-nd/4.0/>).

1. Introduction

The C-shaped load-bearing cartilage tissues in the knee joint, the menisci, carry 50–85% of the mechanical load of the joint [1]. Meniscal tear is the most common soft tissue injury in knee joints, particularly in young and physically active populations [2]. Compared with the outer meniscus (the red zone) that is partially self-healed with the rich blood supply, the middle/inner meniscus tissue (the white zone) has limited self-healing ability, and repairing injured white meniscus remains a clinically challenging problem. The standard treatment is meniscectomy, which removes either partial or total of the damaged tissue and relieves joint pain in the short-term; however, it fails in repairing the tissue in the long-run, inevitably leading to the degenerative joint disease, osteoarthritis [2]. There is an urgent need to better understand how meniscal tissue homeostasis is maintained and how meniscal regeneration may be achieved.

Meniscus is an extracellular matrix (ECM)-rich, dense connective tissue with limited tissue self-repairability, the cell density of tissue resident cells is relatively low (of around 10×10^6 cells per human menisci) [3] and corresponding tissue resident progenitor cells in the inner/white area is around 2.7% of the total meniscal cell population [4]. The meniscus displays nonlinear stress-strain characteristics during load bearing [5]. With its specific semilunar shape and wedge cross-section, the meniscus exhibits a hoop internal ultrastructure, consisting of collagen fiber bundles oriented circumferentially, which convert the weight-bearing axial compression forces into a radially directed force, which is further taken up as circumferential stresses inside, resulting in local tensile stress along the collagen fibers and ECM (Fig. 1a) [6]. The estimated tensile stress-strain in human meniscus is high on a macroscopic scale, which is 50–100 times of the maximum compressive moduli in the axial and radial directions [5,7]. Tensile loading is thus a dominant loading modality in the main body of the meniscus, but how meniscal cells respond to tensile load is not well understood.

The mechanical environment has a profound biological effect on the development and maintenance of cartilage tissues including meniscus [8,9]. Dynamic loading applied to *in vitro* cultured bone marrow derived mesenchymal stem cells (BMSCs) within the range of 5–15% strain stimulated chondrogenic differentiation, characterized by an increase in collagen type II (Col II) production, increased viscoelasticity, and increased glycosaminoglycans (GAGs) production and deposition [10, 11]. On the other hand, overloading abolished these effects, e.g., 20% of cyclic tensile strain reduced cell proliferation, and barely influenced chondrogenic gene expression and ECM production [10]. For *in vitro* three-dimensional (3D) cultures, hydrogel biomaterials, e.g., 10% agarose or methacrylated hyaluronic acid (MeHA), have been used as scaffold to enable daily compressive cyclic loading, e.g., 1 Hz for 4–10 weeks, to the encapsulated cells, which resulted in the induction of a chondrocyte phenotype [12–14]. Cells in meniscus are surrounded by the pericellular matrix (PCM), a narrow cell-matrix interaction zone that has softer mechanical properties compared to the ECM, which prevents cellular overload. The stiffness of PCM is softer on the microscopic scale, evaluated by the atomic force microscopy (AFM) [15], and the elastic modulus in the outer zone is around 150 kPa, while in the inner region is around 28 kPa (Fig. 1b) [15]. Physiological mechanical loading in meniscus could maintain cellular ECM biosynthesis [16–18], establish tissue patterns and fine structures [19], and promote maturation of the engineered fibrocartilage constructs after transplantation [18,20].

Endogenous tissue-resident stem/progenitor cells are known as one of the cell sources important for tissue homeostasis. Similar to BMSCs, human meniscus stem/progenitor cells (hMeSPCs) can be isolated and selected on the basis of their colony forming ability [21–23], and are characterized by positive expression of MSC-associated cell surface markers, such as CD73, CD90 and CD105 [24]. Our previous work has demonstrated the existence of endogenous progenitor cells in meniscus [25]. More recently, meniscus progenitor subpopulations have been

identified by single-cell RNA sequencing, and were characterized by high clonogenicity properties and expression of cell surface markers of CD146⁺ and MYLK⁺ [4]. hMeSPCs showed more meniscal tissue-specific activities compared to hBMSCs, including higher clonogenicity, higher expression level of Col II, and lower expression level of collagen type I (Col I) [22,26].

Given the load-bearing function of the meniscus and the potential role of hMeSPCs in meniscus homeostasis, a better understanding of the mechanobiological responses of hMeSPCs towards biomimetic loading could provide new insights for *in situ* meniscus repair and meniscus tissue regeneration (Fig. 1a). In this study, we adopted a hydrogel scaffold to fabricate a 3D construct to study the mechanobiological properties of encapsulated hMeSPCs. Photocrosslinkable gelatin methacryloyl (GelMA) hydrogels have been widely applied in cartilage tissue engineering [27,28] and cell-based therapies as a delivery vehicle for living cells [29] or bioactive factors [30]. The mechanical properties of the GelMA hydrogel can be fine-tuned based on hydrogel concentration, photo-exposure time, and degree of substitution (DS) to enable the application of biomimetic loading to encapsulate cells similar to that present in native tissues [31]. We first designed and assembled a GelMA hydrogel-based mechanical actuator capable of applying physiologically relevant tensile strain (10% tensile strain, 0.5 Hz) to hMeSPCs in the 3D cultured milieu. With this set-up, we analyzed: (i) the mechanobiological response of 3D encapsulated hMeSPCs under physiologically relevant mechanical stimulation; (ii) the effect of mechanical loading on GelMA degradation and cell-derived ECM accumulation; and (iii) the influence of mechanical stimulations on the dynamic of ECM homeostasis. Our findings have provided insights on the influence of mechanical stimuli on the function and cellular bioactivity of the meniscus.

2. Materials and methods

Isolation and expansion of human meniscal cells: Human meniscus specimens (Table S1) were obtained from patients undergoing total knee arthroplasty surgeries (inclusion criteria: patients undergo knee arthroplasty; exclusion criteria: patients with infectious disease, patients with musculoskeletal tumors), with approval from The Chinese University of Hong Kong Clinical Research Ethics Committee (NTEC-CUHK Ref. 2019. 078). Human primary meniscal cells were isolated from the digested tissue after overnight incubation with 0.2% collagenase I (Gibco, Grand Island, NY, USA). Following isolation, cells were expanded on tissue culture plastic in low-glucose Dulbecco's Modified Eagle's Medium (DMEM) supplemented with 1% antibiotics-antimycotic and 10% fetal bovine serum (FBS) (all materials obtained from Invitrogen, Carlsbad, CA, USA), and were cultured at 37 °C with medium change every 2–3 days. To minimize donor-associated differences, the isolated meniscal cells were subsequently pooled into 3 batches (3 age and gender matched biological donors per batch at a cell density ratio of 1: 1: 1, Table S1). Passage 2–4 cells of each batch were used for the selection of progenitor cells.

Colony formation assay: To select hMeSPCs, isolated primary meniscal cells in each batch were seeded at low density (10 cells/cm²) in T175 flasks. Fourteen days after initial seeding, individual colonies formed. The colony-forming cells, designated as meniscus progenitor cells [22], were collected and stocked in liquid nitrogen, and were used after passage 3–5 for further experiments. To evaluate the influence of static and loaded culture regimens on the colony forming ability of hMeSPCs, cells were isolated after 15 days from cultures on 2D plastic, and in 3D hydrogel constructs under static and loaded conditions and seeded at low-density in 10-cm culture dishes. At day 14 after seeding, the cultures were stained with 1% Crystal Violet solution (Sigma-Aldrich, St. Louis, MO, USA) for 30 min. After rinsing with phosphate-buffered saline (PBS), the stained colonies were counted. Colony forming units (CFUs) were determined by normalizing the number of colonies to the initial number of seeded cells and expressed as a percentage.

Fabrication of GelMA constructs and hMeSPCs encapsulation: GelMA

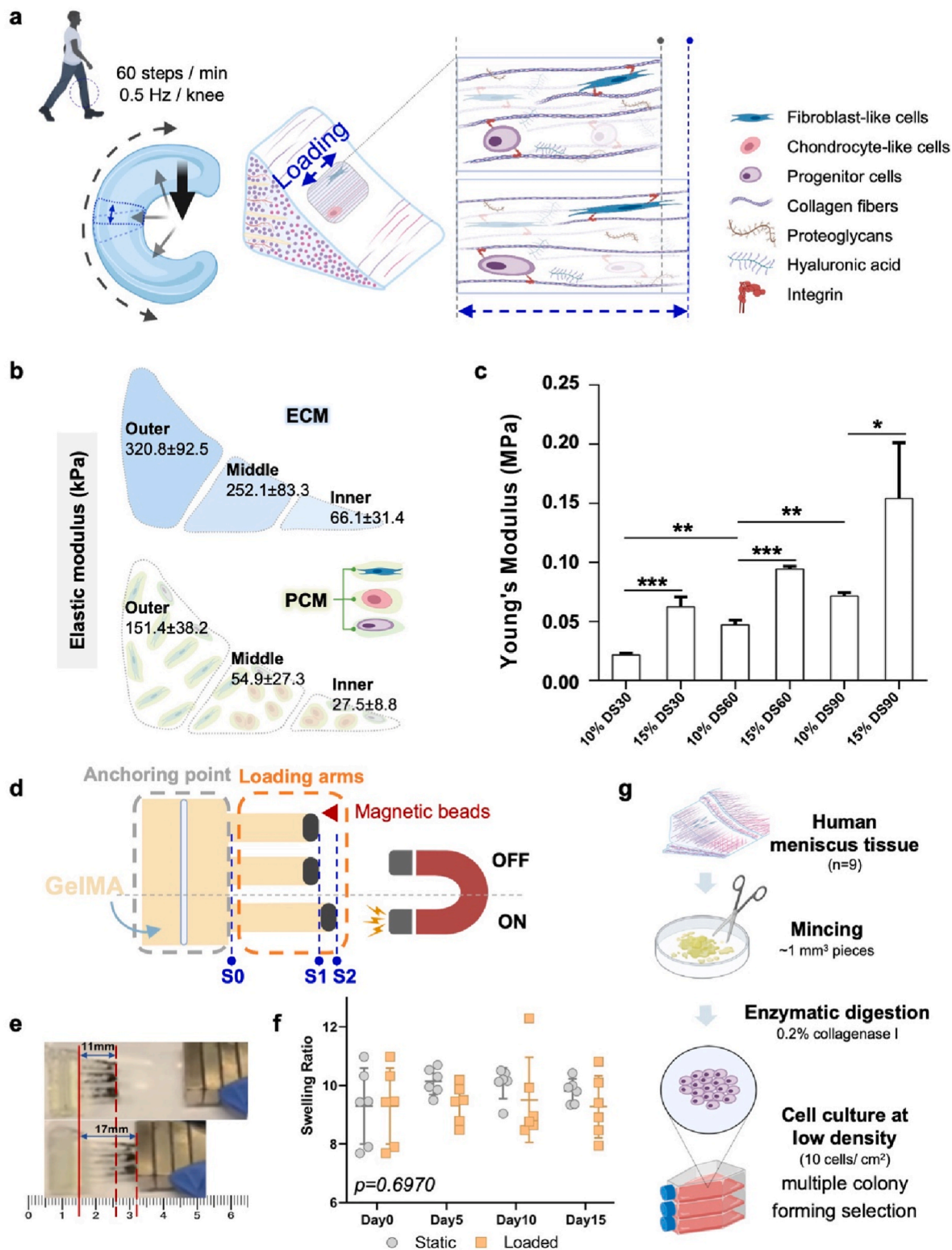


Fig. 1. Design and application of GelMA-based mechanical actuator to provide biomimetic cyclic tensile loading to hydrogel-encapsulated hMeSPCs. (a) Diagrammatic representation of tensile loading in the native meniscal resident cells in the load-bearing joint, specifically showing joint load-bearing of meniscus tissue at a "slow walk" speed. (b) Elastic moduli of the ECM and PCM of various regions of the native porcine meniscus at the microscopic level, evaluated by AFM; data adopted from Ref. [15]. (c) Young's modulus values of 10% and 15% w/v GelMA with 30%, 60%, and 90% DS. *, $p < 0.05$; **, $p < 0.01$; ***, $p < 0.001$. Data are mean ± SD, $n \geq 6$. (d) Operating principle of the actuator. Anchoring point: big block of GelMA with anchor to fix the whole hydrogel construct in the cell culture plate in a certain position; Loading arms: GelMA hydrogel with/without cells can be loaded in the loading arms, and the magnetic beads are loaded in the end of the loading arms; S0, loading arms fixation point; S1, the end position of loading arms without the influence of magnetic field; S2, hydrogel elongation position when the magnetic field is applied; a photo of the actuator can be found in [Supplementary Fig. S2](#). (e) Picture of the GelMA constructs: GelMA hydrogel elongation in response to external magnetic stimuli to provide cyclic tensile loading on the loading arms. (f) Swelling ratio of the GelMA hydrogel (10% w/v, 60% DS) under static and loading conditions at days 0, 5, 10, and 15. (g) Harvesting strategy for hMeSPCs.

hydrogel was dissolved in 0.25% lithium phenyl-2,4,6-trimethylbenzoylphosphinate (LAP) solution (both reagents obtained from Engineering For Life, Zhejiang, China). The GelMA actuator was constructed using a polydimethylsiloxane (PDMS) casting mold custom-built using soft lithography, consisting of one anchoring point (L × W × H: 20 mm × 7 mm × 6 mm), three loading arms (L × W × H: 10 mm × 3 mm × 1.5 mm), with 6 mg of 50–100 μm diameter embedded at the free end of each arm. hMeSPCs were encapsulated in the loading arms in a concentration of 5×10^6 cells/ml and the hydrogel constructs were photocrosslinked by exposure to 405 nm UV light for 25–30 s. The GelMA actuators with or without hMeSPCs encapsulation were cultured in 35-mm culture dishes in high glucose DMEM with 1% antibiotics-antimycotic and 1% insulin-transferrin-selenium-X (all obtained from Invitrogen, Carlsbad, CA, USA) at 37 °C, with medium change every other day.

Mechanical stimulation: The GelMA hydrogel constructs with or without encapsulated hMeSPCs were precultured for 24 h, followed by tensile mechanical stimulation, with statically cultured groups serving as control. Intermittent cyclic tensile loading was introduced using a magnetically-equipped automated motion of 0.5 Hz frequency for 1 h/day up to 15 days. The GelMA actuators were precisely controlled to move cyclically towards and away from the fixed magnets (2902 Gauss magnetic field in each magnet), achieving 10% elongation of the arms. All cultures, both static and loaded, were maintained in the incubator at 37 °C, 5% CO₂, and were collected for analysis at days 0, 5, 10, and 15. The GelMA constructs were fixed in the culture dish, and the loading arms can achieve 10% elongation in such position. Considering the GelMA hydrogel degradation, the mechanical properties changes and hydrogel deformation, the fixation position of GelMA construct in the culture dish was adjusted before daily mechanical stimulation.

Tensile testing: Tensile testing was performed using a clamps-modified rheometer (Kinexus system, model: KNX2110, Malvern Instruments Ltd., Worcestershire, UK) to determine the mechanical property of the GelMA hydrogel. At least six hydrogel constructs (3 mm wide × 1.5 mm thick × 10 mm long) were evaluated for each group, and the test was conducted at an extension speed of 1 mm/s to record the tensile force. For optimization of hydrogel composition for 3D culture, the Young's modulus values of 10% and 15% w/v GelMA hydrogels with 30%, 60%, and 90% DS were determined. To assess hydrogel degradation during culture, the Young's modulus values of GelMA hydrogel constructs with or without encapsulated hMeSPCs under static and loaded regimens were determined at days 0, 5, 10, and 15.

Swelling test: The swelling property of the GelMA hydrogel (10% w/v, 60% DS) was evaluated by weighing method. Six arms were prepared in each group. Immediately after GelMA formation, each sample was precultured in culture medium in incubator (37 °C, 5% CO₂) for 24 h. After static and loaded cultures at days 0, 5, 10, and 15, the weight of the swollen hydrogel was recorded as wet weight. Then, the hydrogel was lyophilized to obtain dry weight. The swelling ratio can be calculated by the following formula:

$$\text{swelling ratio} = \frac{\text{wet weight} - \text{dry weight}}{\text{dry weight}} \times 100\%$$

Cell viability assay: LIVE/DEAD staining was performed to assess the viability of the GelMA-encapsulated hMeSPCs under static and loaded cultures, which showed live cells stained green by calcein AM and dead cells stained red by ethidium homodimer-1 (EthD-1) (Thermo Fisher Scientific, Waltham, Massachusetts, USA). Constructs were stained in a mixture of 2 μM calcein AM and 2 μM EthD-1 in DMEM for 1 h at 37 °C, followed by rinsing in PBS. Images were captured at days 0, 5, 10, and 15 using Olympus IX83 Inverted Microscope with ZDC (Olympus, Shinjuku, Tokyo, Japan).

To quantify cell viability, hMeSPCs were released on day 15 from cultures maintained on 2D plastic, and from 3D cultures under static and loaded cultures, and were processed for flow cytometry. Cells cultured on plastic were released with trypsin (0.5%, 3 min incubation), while

GelMA encapsulated hMeSPCs were released by incubating the hydrogel constructs in 1 mg/ml collagenase I solution for 1 h at 37 °C. The collected cells were stained with propidium iodide (PI) (1 mg/ml solution in water; 1:500; Invitrogen, Carlsbad, CA, USA) for 15 min at room temperature, and analyzed by flow cytometry using the BD LSR Fortessa Cell Analyzer (BD Biosciences, San Jose, CA).

Cell morphology assessment: The morphology of GelMA-encapsulated hMeSPCs maintained under static and loaded conditions was examined by fluorescence staining of cellular F-actin at days 0, 5, 10, and 15. In brief, the hMeSPCs-encapsulated arms were collected, fixed in 4% paraformaldehyde (PFA), and incubated with Phalloidin-iFluor 555 reagent (1:1000 dilution in 1% BSA; Abcam, Cambridge, UK) for 1 h in the dark, followed by co-staining with DAPI (1:2000 dilution in water; Abcam, Cambridge, UK) for 15 min. Images were captured using the Olympus FV1200 Inverted Confocal Microscope with SIM scanner (Olympus, Shinjuku, Tokyo, Japan). Cell shape was assessed as the cross-section aspect ratio estimated from dimensions of the actin cytoskeleton stained hMeSPCs measured with Image J (National Institutes of Health, USA), and calculated as a ratio of major axis to minor axis.

Analysis of cell surface markers: Flow cytometry was performed to assess the presence of surface markers in hMeSPCs after 15 days of culture on 2D plastic, and in 3D hydrogel under static and cyclic loaded conditions. Immunostaining of hMeSPCs released from each group was carried out first with primary antibodies (1.0×10^6 cells for each) for 30 min, including CD44 (1:200; ab157107), CD29 (1:200; ab24693), CD49e (1:20; ab150361), CD73 (10 μl per 10^6 cells; ab257311), CD90 (10 μl per 10^6 cells; ab23894), and CD105 (1:200; ab114052) (all antibodies obtained from Abcam, Cambridge, UK), followed by Alexa Fluor® goat anti-mouse polyclonal secondary antibody (ThermoFisher, Massachusetts, US). The stained cells were analyzed by flow cytometry as described above.

ECM detection: Histology and immunohistochemistry were used to assess ECM secreted production by GelMA-encapsulated hMeSPCs under static and loaded culture conditions at days 0, 5, 10, and 15. hMeSPCs-GelMA constructs were cryosectioned (10 μm thickness) and stained with Safranin O for histological detection of matrix sulfated glycosaminoglycans (GAGs) to assess proteoglycan production. The presence of Col I and Col II was detected immunohistochemically. The cryosections were first incubated with primary antibodies against Col I (1:500 dilution in blocking buffer; Abcam, Cambridge, UK) or Col II (1:200 dilution in blocking buffer; Merck Millipore, Burlington, Massachusetts, USA) for 30 min at room temperature, followed by incubation with HRP-conjugated secondary antibodies (1:1000 dilution in blocking buffer; Abcam, Cambridge, UK) for 30 min. Detection of immunostaining was done using Pierce™ Peroxidase IHC Detection Kit (Thermo Fisher Scientific, Waltham, Massachusetts, USA) according to the manufacturer's instruction. All images were acquired using Nikon Ni-U Eclipse Upright Microscope (Nikon, Tokyo, Japan). The percentage of the positive stain area was quantified by Image J (NIH, US).

Histological assessment of GelMA degradation: Cryosections of GelMA hydrogel constructs with or without encapsulated hMeSPCs cultured under static and loaded conditions were stained with Picrosirius Red (red, thick collagen fibers; and pink, thin collagen fibers). Images were captured using Nikon Ni-U Eclipse Upright Microscope (Nikon, Tokyo, Japan) at days 0, 5, 10, and 15. The number and size distribution of the pores were estimated using Image J, and total pore area and porosity (total pore area/total area × 100%) were calculated.

Non-invasive assessment of GelMA degradation: Green fluorescence-tagged (GFT) GelMA (Engineering For Life, EFL, Zhejiang, China) was used instead of GelMA to fabricate the 3D hydrogel constructs to visualize matrix degradation during culture under both static and loaded conditions. Fluorescence images were captured at days 0, 5, 10, and 15 using the Olympus FV1200 Inverted Confocal Microscope with SIM scanner (Olympus, Shinjuku, Tokyo, Japan). The fluorescence intensity of the imaged GFT-GelMA hydrogel was converted into a heatmap using Image J.

Real time monitoring and quantification of GFT-GelMA degradation was carried out by measuring the amount of GFT-GelMA degradation product released into the culture medium. The culture medium of the GFT-GelMA constructs with or without encapsulated hMeSPCs and cultured under static and loaded conditions was collected daily, and the fluorescence intensity of released soluble GFT-GelMA by-products measured (excitation 492 nm; emission 568 nm) using Molecular Devices SpectraMax i3X Multimode Microplate Reader (Molecular Devices, LLC, San Jose, CA).

Transcriptome and gene expression analysis: hMeSPCs were released from cultures maintained for 15 days on 2D plastic, and in 3D hydrogel under static and cyclic loading conditions, and total RNAs were isolated by extraction with TRIzol, followed by purification using RNeasy® Mini kit (Qiagen, Hilden, Germany) according to the manufacturer's instruction. Total RNA concentration was quantified spectrophotometrically using Nanodrop Spectrophotometer 2000 (Thermo Fisher Scientific, Waltham, Massachusetts, USA). Gene expression profiles were analyzed by RNA sequencing (BGI, Shenzhen, Guangdong, China), and further analysis was performed by means of the related software Dr. Tom (BGI, Shenzhen, Guangdong, China).

Statistical analysis: Statistical analysis was performed using GraphPad Prism software (version 7; GraphPad, CA, USA). All data were presented as mean \pm SD. Student's *t*-test was performed on experiments containing two groups. Analysis of variance (ANOVA) (one-way ANOVA for one independent variable, two-way ANOVA for multiple variables) and post hoc analysis (Dunnett's Multiple Comparison test or Tukey test) were used for analysis of data from experiments with more than two experimental groups that required comparisons between every group. All experiments were performed with at least 2 batches of biological donors ($N \geq 6$, 3 biological donors were pooled as 1 batch, and total 3 batches of cells were used for most experiments unless stated specifically, i.e. $N = 9$), and at least 3 technical repeats were carried out in all experiments. Error bars illustrate 1 standard deviation of the mean. A *p*-value smaller or equal to 0.05 was considered statistically significant.

3. Results and discussion

3.1. *In vitro* application of biomimetic cyclic tensile loading to hMeSPCs with GelMA hydrogel-based actuator

To simulate the tensile stimulation to the meniscal cells by the frequency and duration of a "slow walk" at low daily activity levels, the GelMA formulation was optimized to support *in vitro* cell growth as well as biomimetic tensile loading of hMeSPCs at a frequency of 0.5 Hz per knee (60 steps/min; 1 h/day; Fig. 1a) and 10% strain, based in part on previous reports that cellular chondrogenic effects were found in agarose and MeHA hydrogel with 10% strain of compressive loading [32–36]. For GelMA formulation, we took into consideration the reported mechanical properties of the ECM and PCM of native meniscus, previously evaluated and identified by atomic force microscopy with porcine meniscus, i.e., ~60 kPa for inner ECM and middle PCM (Fig. 1b) [15,37,38]. Because the inner white-zone of meniscus is avascular, aneural and alymphatic, lesions located in the inner and middle part of the meniscus have limited healing capacity, in this study, the GelMA hydrogel used for hMeSPC encapsulation in the actuator was optimized to 10% w/v with a 60% DS, which possessed a mean Young's modulus of 47.5 kPa (Fig. 1c, from concentrations: 10% and 15% w/v; DS: 30%, 60%, 90%, respectively), to match the mechanical properties of native inner meniscus ECM at the microscopic level [37,38].

GelMA hydrogel-based constructs to be subjected to cyclic tensile loading were assembled as shown in Fig. 1d, showing one anchoring point for positional fixation, and three loading arms filled with magnetic beads to respond to the external magnetic stimuli. The loading arms were elongated as a result of response to the external magnetic stimuli (ON in Fig. 1d) and restored once the magnets moved away (OFF in Fig. 1d), with the maximum elongation estimated to be up to 54.5%

(Fig. 1e). Combined with automated motion, the actuator allowed precise control of the parameters of cyclic loading, including both frequency and magnitude, to the GelMA hydrogel arms, that were on par with commercially available bioreactors [18,20,39,40], while permitting contactless elongation and simultaneous 3D cultivation of loaded cells. This set-up thus overcame the problems of sample fixation and hydrogel substrate damage in other 2D [3] and clamps-based 3D bioreactors [41–43], and no significant swelling difference was observed in the GelMA construct under tensile loading, compared to static cultures (Fig. 1f).

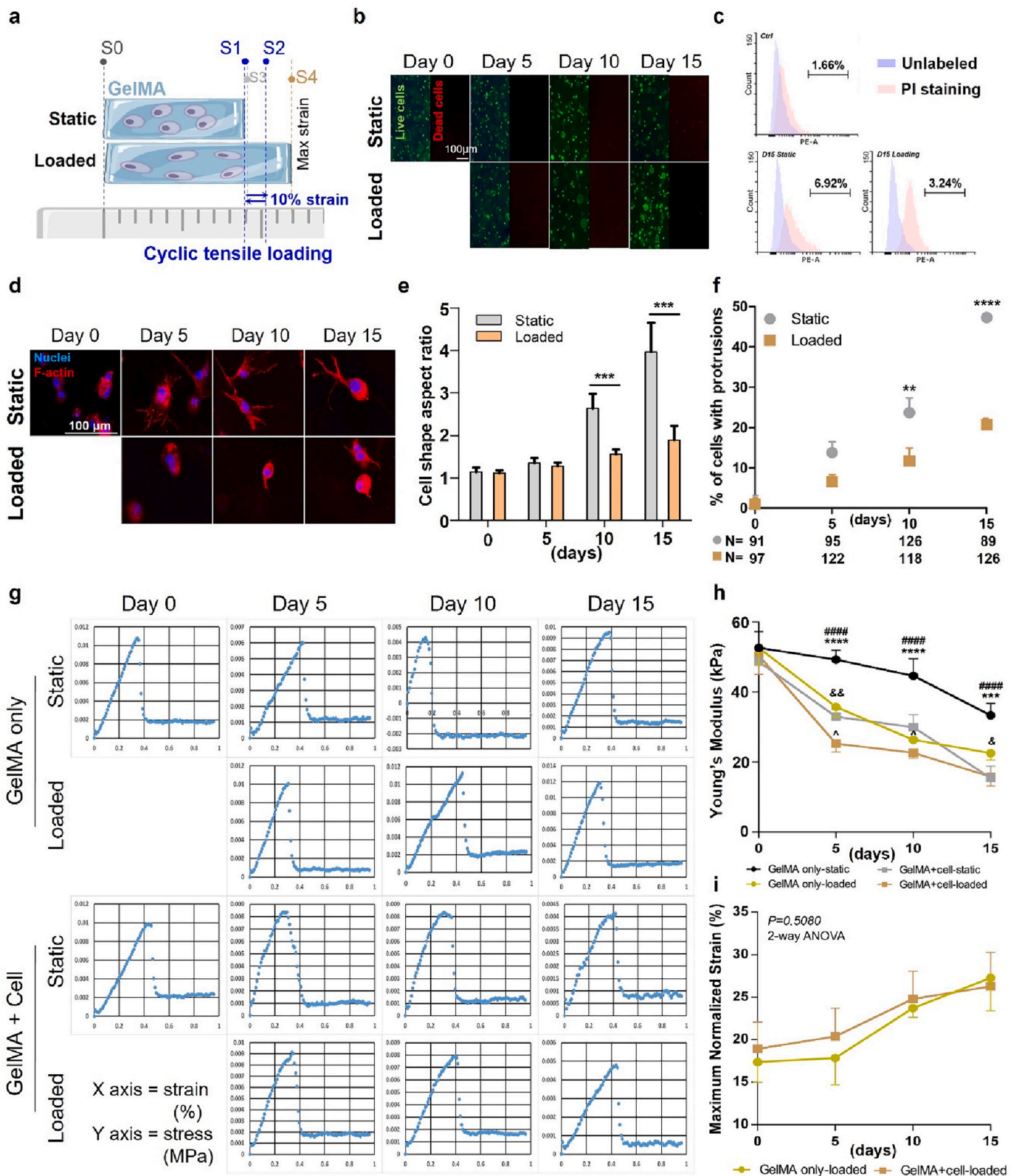
Next, hMeSPCs, tissue-resident stem/progenitor cells of human meniscus, were collected and analyzed using the actuator for their mechanobiological responses in terms of growth factor generation and matrix deposition, important criteria of meniscus regeneration *in situ* [22]. In brief, hMeSPCs were isolated and collected from the primary meniscal cells ($n = 9$ biological donors) on the basis of colony formation assay (Fig. 1g) [22], and their nature confirmed on the basis of positive expression of MSC-like surface markers (Fig. S1). The hMeSPCs (pooled into three batches: batch1, B1, from 65 M/56F/77F; batch 2, B2, from 76 M/73F/59F; and batch 3, B3, from 77 M/66F/65F) were then encapsulated in the loading arms of photocrosslinked GelMA construct (Fig. 1d) and loaded in the actuator, and the constructs subjected to mechanical stimulation with repetitive elongation and restoration of GelMA hydrogel according to specific parameters.

3.2. Cell viability, morphology, and mechanical properties of hMeSPCs-GelMA constructs after mechanical loading

To recapitulate the physiological tensile microenvironment of native meniscal cells *in vitro*, we adopted cyclic tensile loading of the hMeSPCs-GelMA constructs (5×10^6 cells/ml) at 10% strain (S1–S2 in Fig. 2a) and a frequency of 0.5 Hz for 1 h/day to match mild daily body activity such as a slow walk (Fig. 1a). Cell viability of hMeSPCs in the constructs loaded with actuators was assessed by LIVE/DEAD staining every 5 days until day 15 (Fig. 2b). High viability of hMeSPCs was maintained at all time points in both the static and loaded cultures. Flow cytometry was also used to quantify cell viability by PI staining of hMeSPCs released from GelMA hydrogel after 15 days of loading, showing cell viability rate of 96.76% in 3D loaded group, 93.08% in 3D static group, and 98.34% in monolayer cultures (Fig. 2c). This non-cytotoxicity in cell-GelMA hydrogel cultures observed here was in line with earlier reports [44,45]. In addition, the maintenance of high cell viability in the hMeSPC constructs after cyclic tensile loading suggested that the loading regimen applied, i.e., 0–12% in elongation and 0.01–1 Hz, formulated to be physiologically mimetic [12–14], was indeed biocompatible.

Morphologically, cyclic tensile loading groups resulted in more cells exhibiting a rounded/elliptical shape, while cells with a more extended shape were seen in the static groups (Fig. 2d). Morphometric analysis showed an overall increase in cell shape aspect ratio with increasing culture time, suggesting progressive spreading of the hydrogel encapsulated cells; on the other hand, cyclic tensile loading resulted in significantly lower aspect ratios at day 10 ($p < 0.001$) and day 15 ($p < 0.001$), indicating a more spherical morphology (Fig. 2e). The percentage of cells with protrusions is higher in static group than the hMeSPCs under loaded condition, especially at day 10 ($p < 0.01$) and day 15 ($p < 0.0001$) (Fig. 2f). It is noteworthy that the more spherical cell shape is similar to that of cells in the inner region of healthy meniscus *in situ* [46, 47], and is consistent with the morphology of chondrocytes encapsulated in 3D hydrogel *in vitro* [10,48–50].

After 15 days of cyclic loading (S1–S2 in Fig. 2a), the Young's modulus values of all GelMA constructs decreased from 47 kPa to 20 kPa, and the length of GelMA constructs (S0–S3 in Fig. 2a) slightly increased (Fig. S3), likely reflecting GelMA hydrogel swelling and degradation during culture (Fig. 2g and h). In parallel, the maximum elongation of these hydrogel constructs (S3–S4 in Fig. 2a) increased during 15 days of culture period (Fig. 2i). GelMA constructs retained



(caption on next page)

Fig. 2. Cell viability, cell morphology, and mechanical property of hMeSPC-GelMA constructs after mechanical loading. (a) Mechanical loading regimen for GelMA hydrogel, consisting of 10% elongation under cyclic loading. S0, fixation point; S1, starting point; S2, 10% hydrogel elongation, at which point the tensile load drops off and the hydrogel starts to restore to the relaxation point, S3; S4, maximum elongation point, where the loading arms are maximally elongated in response to magnetic force at this point. (b) LIVE/DEAD staining of hMeSPCs encapsulated in GelMA hydrogel (10% w/v, 60% DS) after static culture and tensile loading at days 0, 5, 10, 15. Left panel: green, live cells; right panel: red, dead cells. Scale bar = 100 μm . (c) Flow cytometric analysis of PI stained hMeSPCs released after 2D culture (Ctrl), and 3D cultures maintained under static (Static), and tensile loading (Loaded, 10% elongation, 0.5 Hz, 1 h/day) conditions at day 15. The % of dead cells are estimated based on the relative number of PI positive cells in the total population. 3 batches ($n = 9$ biological donors) were examined with 3 technical repeats. Representative data from 1 batch is shown. (d) Representative images of cytoskeletal morphology (F-actin, phalloidin-iFluor 555 staining, red; nuclei, DAPI staining, blue). (e) Cross-sectional cell shape aspect ratio of the encapsulated hMeSPCs under static and loaded conditions at days 0, 5, 10, 15. Data were analyzed by ANOVA; $***, p < 0.001$ between static and loaded groups at days 10 and 15. Data are mean \pm SD; $n = 8$ random views from high magnification field (HMF) per group. (f) Quantification of protrusions in hMeSPCs under static and loaded conditions at days 0, 5, 10, and 15. $N =$ the number of counted cells in hydrogel. Data are mean \pm SD, analyzed by ANOVA; $** , p < 0.01$ and $**** , p < 0.0001$ between static and loaded groups at days 10 and 15, respectively. (g) Representative pictures of stress-strain curves of GelMA constructs with or without encapsulated hMeSPCs, maintained under static and loaded conditions at days 0, 5, 10, 15. Data were collected from $n = 3$ batches with total of 9 biological donors; each experiment was performed with triplicates as technical repeats. The X axis is strain, and the number represent length change (mm)/original length (mm), and the Y axis is stress (MPa). (h) Young's modulus values of GelMA constructs with or without encapsulated hMeSPCs, maintained under static and loaded conditions at days 0, 5, 10, 15. Data were collected from $n = 3$ batches with total of 9 biological donors; each experiment was performed with triplicates as technical repeats. Two-way ANOVA with post-hoc was used to study the difference between groups; Data are mean \pm SD. GelMA only-Loaded groups vs GelMA only-Static groups: $***, p < 0.001$ and $****, p < 0.0001$; GelMA + cell-Loaded groups vs GelMA + cell-Static groups: $^{\circ}, p < 0.05$; GelMA + cell-Static groups vs GelMA only-Static groups: $####, p < 0.0001$; GelMA + cell-Loaded groups vs GelMA only-Loaded groups: $^{\text{A}}, p < 0.05$ and $^{\text{A}\text{A}}, p < 0.01$. (i) Maximum elongation (S3–S4) of GelMA hydrogel cultures at days 5, 10, and 15 after loading, normalized to initial length of GelMA-hydrogel arms (S0–S3). Two-way ANOVA: $^{\circ}, p < 0.05$ between day 15 and day 0 in GelMA only group; and $^{\#}, p < 0.05$ between day 15 and day 5 in GelMA only group. Data were collected from $n = 3$ batches with a total of 9 biological donors; each experiment was performed with triplicates as technical repeats.

26.28% of maximum normalized strain, while hMeSPC-encapsulated GelMA constructs retained 27.28%, an increase of $\sim 10\%$ compared to the respective day 0 strain values, 17.36% and 18.94% (S1–S4 in Fig. 2a). No significant difference was found in the maximum normalized strain between cell-encapsulated constructs and GelMA-only constructs, suggesting that the mechanical properties of the GelMA constructs were not compromised by cell encapsulation and could withstand 15 days of tensile loading without further damage (see histological results in Fig. S4).

3.3. Gene clusters modulated by intermittent cyclic tensile loading in hMeSPCs

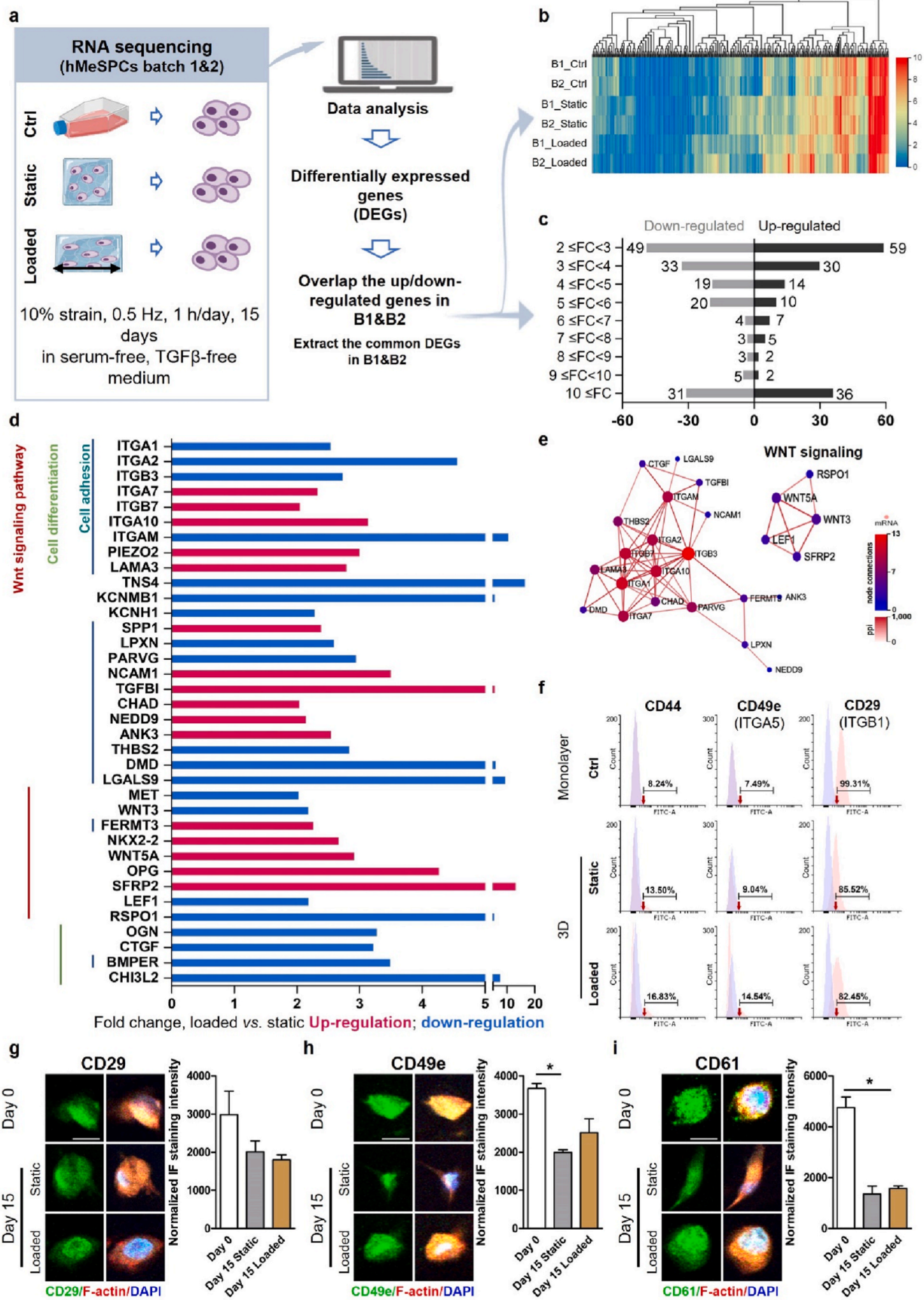
After 15 days of static or loaded culture in the above actuator (10% elongation, 0.5 Hz, 1 h/day), the hMeSPCs encapsulated in GelMA hydrogel can be altered in many ways. To observe the influence of mechanical forces on these cells, the transcriptome is firstly analyzed (Fig. 3, Control: cells under 2D monolayer culture; Static: cells in GelMA hydrogel without loading; Loaded: loaded cell-GelMA culture), and a total of 332 genes were identified to be responsive to the intermittent cyclic tensile stimulation by transcriptome analysis (Fig. 3b, static culture vs loaded culture), including 165 up-regulated genes and 167 down-regulated genes that were segmented based on the average absolute fold change (FC) (Fig. 3c). It is noteworthy that the cell-GelMA constructs were cultured in a serum-free, transforming growth factor- β (TGF- β)-free medium, thus excluding potential influence of serum and TGF- β on hMeSPCs, and highlighting the effects of tensile loading.

A number of gene clusters were identified among the differentially regulated genes as a result of the mild mechanical loading (Fig. 3d and e). Among the identified genes, integrins, including *ITGA1*, *ITGA2*, *ITGB3*, *ITGB7* and *ITGA10* were predicted as key players in the PPI network analysis (Fig. 3e), suggesting enhanced cell-matrix interaction by mechanical loading. Integrins are the principle cellular receptors to bind to ECM, integrin $\alpha 5\beta 1$ and $\alpha V\beta 3$ act as receptors of fibronectin and have great roles in chondrocyte mechanoresponsive and cartilage regeneration [51,52]. To confirm the enhanced cell-matrix integration, we then evaluated the expression of the known cartilage ECM receptors, CD44 (a hyaluronan receptor), CD49e (ITGA5), and CD29 (ITGB1). The protein expression levels of CD44, CD49e (ITGA5), and CD29 (ITGB1) was assessed by flow cytometry (Fig. 3f). The loading induced increase in CD49e, i.e., integrin $\alpha 5$ (monolayer culture, 7.49%; static group, 9.04%; and loaded group, 14.54%), taken together with the continued high expression of CD29, i.e., integrin $\beta 1$ (monolayer culture, 99.31%; static group, 85.52%; and loaded group, 82.45%), could represent

increased formation of the $\alpha 5\beta 1$ integrin, the classic fibronectin receptor also present in chondrocytes [53–55], to act as a mechanical signal transducer between the ECM and chondrocytes [56]. These flow cytometry results corroborated the gene expression profile results from transcriptome analysis (Fig. 3d).

In addition, the protein-protein interaction (PPI) network analysis indicated *ITGB3* as a core gene interacting with most other genes in the mechanical sensitivity gene cluster (Fig. 3e), and the fluorescent intensity of integrin proteins ITGB1 (CD29), ITGA5 (CD49e), and ITGB3 (CD61) in positive stained cells were quantified and normalized by immunostaining (Fig. 3g–i). Taken together with the increased cell surface expression of CD49e, i.e., integrin α , it is likely that loading enhances formation of the $\alpha V\beta 3$ integrin complex, which has been shown to play an important role in cell-matrix interaction and maintenance of joint tissue homeostasis [57].

Genes involved in Wnt signaling pathway activation were also identified in the mechanically sensitive gene cluster. We observed the gene changes of *WNT5A*, *WNT3*, *FGF18*, *LEF1*, *SFRP2*, *FERMT3*, and *RSPO1* induced by mechanical loading (Fig. 3d). Among these 7 genes, *WNT5A* was slightly increased with a fold change less than 3, suggesting a potential activation of noncanonical Wnt/calcium pathway by the mild loading, and it is in line with its reported function in chondrocyte cytoskeletal remodeling [58,59]. *WNT3* was upregulated for 2 folds, and it relates to a fibroblastic like phenotype in chondrocytes [60], and represses the ECM gene production of chondrocytes under tensile strain (7.5%, 1 Hz, 0.5 h) [61]. Meanwhile, the WNT signaling target and regulating gene of *FGF18* was upregulated around 4 folds (Fig. 4e), indicating the activation of canonical Wnt signaling. On the other hand, the changes of *LEF1*, *SFRP2*, *FERMT3*, and *RSPO1* in WNT signaling with biological function in cartilage and chondrocytes pointed to a direction of chondrogenesis and chondro-protection. *Lymphoid enhancer factor 1* (*LEF1*) was reduced by 2 folds, and it is a transcription factor that is regulated by β -catenin. *LEF1* is associated with cartilage breakdown and osteoarthritis progression, and could enhance *MMP13* gene expression in human chondrocytes [62]. *Secreted Frizzled-Related Protein 2* (*SFRP2*), a Wnt antagonist, was upregulated for more than 10 folds, and this is in line with previous report that the *SFRP2* was one of the mechanosensitive genes during skeletal and joint tissue development [63]. *FERMT3*, the coding gene of Kindlin-3, was upregulated for >2 folds, and Kindlin-3 expression is enhanced in BMSC chondrogenic differentiation [64]. *Rspodin 1* (*RSPO1*) is an activator of Wnt signaling, and the expression level of *RSPO1* was reduced for more than 5 folds in the loaded group. *RSPO1* is known as a vibration-induced bone-enhancing (vibe) gene, and administration of *Rsp1* protein could rescue osteoporosis in mice model



(caption on next page)

Fig. 3. Transcriptome analysis of hMeSPCs under intermittent tensile loading. (a) Scheme of transcriptome assay and data analysis. 322 differentially expressed genes were identified in response to 15-day mild intermittent cyclic tensile loading. (B1, batch 1: pooled cells from 65 M/56 F/77 F; B2, batch 2: pooled cells from 76 M/73 F/59 F; total of 6 biological donors). **Ctrl, Static, Loaded:** as described in Fig. 2; **FC,** absolute fold change in results from RNA-seq. (b) Heatmap of loading-induced differentially expressed genes in hMeSPCs in B1 and B2 (c) Count of up- and down-regulated genes common to B1 and B2 based on mean FC. (d) Mechanobiological-related gene clusters regulated by intermittent tensile stimulation (loaded vs static; red, up-regulated; blue, down-regulated), and classified by biological function. (e) Protein-protein interaction network of the regulated genes common to B1 and B2, analyzed by Dr. Tom software, min score = 500. (f) Flow cytometry results on expression of CD44, CD49e, CD29 from a representative experiment. (g–i) Representative images (left) and corresponding quantification of the normalized fluorescent intensity (right, normalized to counted cell nuclei) of immunostaining of CD29 (g), CD49e (h), and CD61 (i) in hMeSPCs under static and loaded conditions at days 0 and 15 (CD markers, green; nuclei, blue; F-actin, red). Scale bar = 10 μm. Data are mean ± SD, analyzed by ANOVA; *, $p < 0.05$.

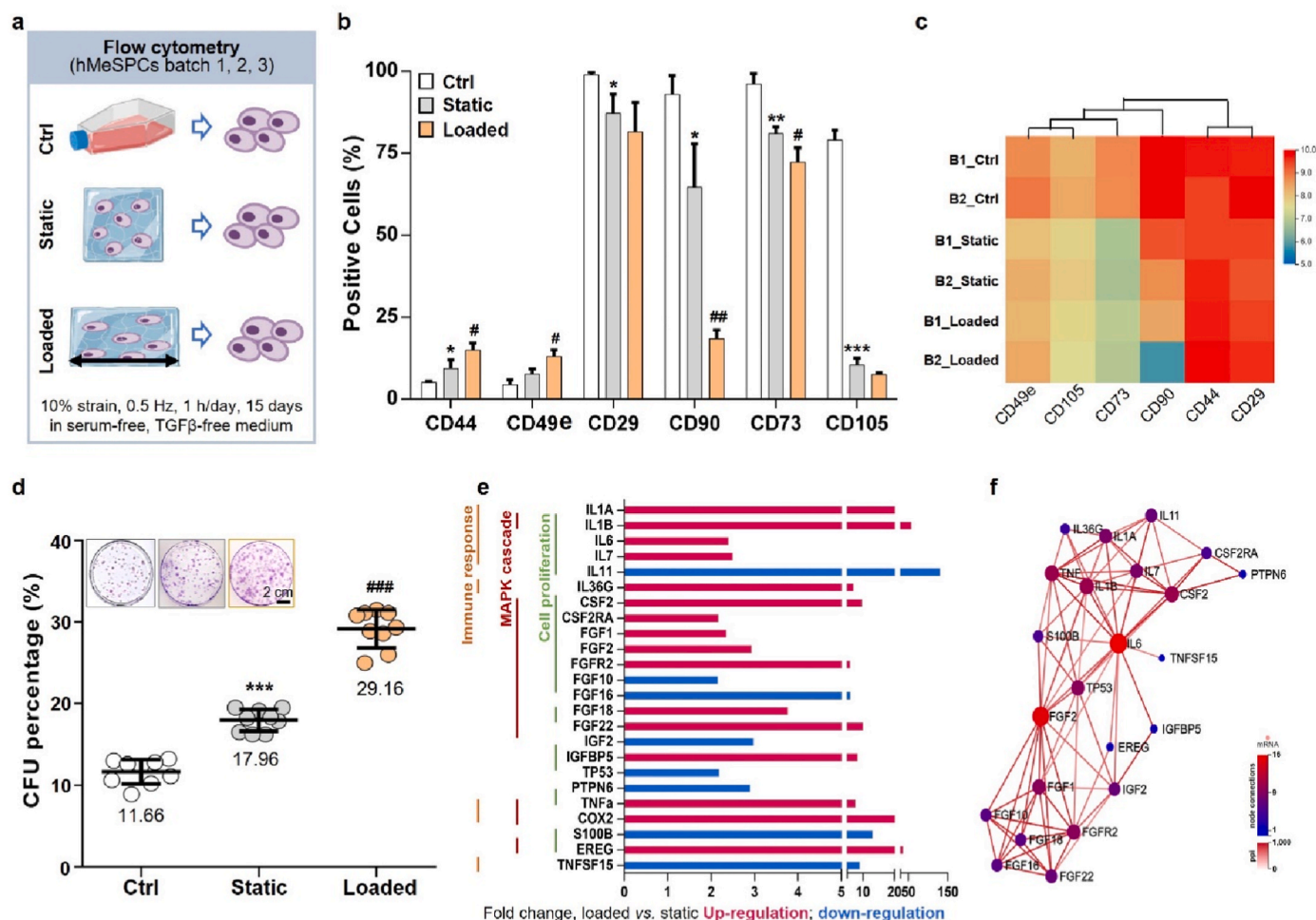


Fig. 4. Biomimetic tensile loading modulates differentiation, self-renewal and senescence characteristics of hMeSPCs. (a) Scheme of flow cytometry assay of hMeSPCs surface marker expression after 15-day culture under 2D (Ctrl), 3D static (Static), and tensile loading (Loaded) conditions. (b) Flow cytometry analysis of the expression of mechano-responsive cell surface markers (CD29, CD49e, CD44) and MSC-associated cell surface markers (CD90, CD105, CD73) in hMeSPCs. *, $p < 0.05$; **, $p < 0.01$; ***, $p < 0.001$ relative to Ctrl; #, $p < 0.05$; ##, $p < 0.01$ relative to Static. Data are mean ± SD values collected from $n = 3$ batches with a total of 9 biological donors; each experiment was performed with at least triplicates as technical repeats. (c) Heatmap representation of the expression levels of the corresponding genes obtained by RNA-seq. (d) Quantification of CFUs in 3D static culture (Static), and tensile loading (Loaded) groups, normalized by initial seeding number of hMeSPCs in 2D culture (Ctrl). One-way ANOVA: ***, $p < 0.001$ relative to Ctrl group; and ###, $p < 0.001$ relative to Static group. Data are mean ± SD values collected from $n = 3$ batches with total of 9 biological donors; each experiment was performed with at least triplicates as technical repeats. (e) Cell senescence-related genes regulated by intermittent tensile stimulation (loaded vs static; red, up-regulated; blue, down-regulated) and classified by biological function, based on transcriptome analysis described in Fig. 3. (f) Protein-protein interaction network of the tensile loading regulated senescence-related genes presented in (e). **B1, B2, B3, Ctrl, Static, Loaded:** as described in Fig. 3.

[65]. The high expression of *RSPO1* was found in osteoarthritic cartilage next to subchondral bone, and represent a molecular interaction in diseased joint [66]. From the above information, although a 2-fold upregulation of *WNT3* and *WNT5A* was observed, we could conclude a potential decrease or inhibition of the canonical Wnt pathway by loading, based on the highly expressed Wnt antagonist (*SFRP2*, >13 fold) and down-regulated Wnt activators (*LEF1*, >2 fold; *RSPO1*, >5 fold).

We also analyzed known cellular mechanotransducers, such as *YAP1*, *PIEZO1/2*, and the recently discovered tropomyosin-1 (*TPM1*) [67], but did not observe strong differences among groups (Table S2). It is possible that, because the RNAseq data are from day 15 of culture, the time frame of detectable expression differences of these genes has passed. Current data are observation of long-term 3D cultures of primary isolated cells and may miss important changes; earlier time points, molecular perturbations, more stable cell lines (such as iPSC derived cell

lines), and genetic manipulations are needed in future study.

3.4. Effect of intermittent cyclic tensile loading of stem cell related characteristics

The expression profile of cell surface MSC markers (i.e., CD90, CD73, and CD105) and mechanosensitive markers (i.e., CD44, CD29, and CD49e) in hMeSPCs was examined by flow cytometry after 15 days of culture (Fig. 4a, b, c). The high level of expression of MSC surface markers in monolayer cultured hMeSPCs (CD90, 92.88%; CD73, 96.08%; CD105, 78.96%) was reduced when in GelMA hydrogel cultures (static groups, CD90, 64.60%; CD73, 81.00%; CD105, 10.35%) and dropped significantly in the loaded groups (CD90, 18.41%; CD73, 72.19%; CD105, 7.42%) (Fig. 4b). The altered expression of these cell surface MSC markers as result of exposure to biomimetic loading suggests initiation of stem cell differentiation under intermittent cyclic tensile loading [68].

On the other hand, biomimetic tensile loading resulted in an increased expression of ECM receptors (Fig. 4b and c). CD44, the hyaluronic acid (HA) receptor, increased by 15 days of loading - monolayer culture control, 8.24%; static group, 13.50%; and loaded group, 16.83%. The alternation of the stem cell surface markers, including the increase in CD44 and a decrease in CD90, CD73 and CD105 in the loaded group, suggested stem cell differentiation, possibly towards chondrogenesis [69,70].

Taken together with the expression profiles of integrins in hMeSPCs under mechanical loading (Fig. 3), the above data strongly suggests that biomimetic intermittent cyclic tensile stimulation of hMeSPCs enhances cell-matrix interaction and support differentiation. We next examined the self-renewal ability of mechanically stimulated hMeSPCs by carrying out colony formation assay of cells released from the GelMA constructs after 15 days of loading. First, no significant difference in total cell count was found among the different groups of hMeSPCs (Fig. S5), suggesting that cyclic loading did not change cell proliferation in hydrogel. On the other hand, 3D hydrogel culture resulted in significantly increased colony forming ability of the released hMeSPCs, as seen in both 3D static and loaded cultures (Fig. 4d). The number of colony forming units (CFUs) was higher in 3D cultures (Static group: $17.96 \pm 1.34\%$), and even higher in loaded groups ($29.16 \pm 2.33\%$), compared to $11.66 \pm 1.51\%$ in 2D monolayer control culture. The observed increase in CFUs caused by the intermittent cyclic tensile loading suggests a supportive role of mechanical loading in hMeSPC replication and self-renewal. Furthermore, transcriptomic analysis showed the clustering of a group of cell senescence-related genes (Fig. 4e). The increased expression of *IL1A*, *IL1B*, *IL6*, *IL11* and *COX2* suggested a special cell inflammatory response pattern in the biomimetic loading groups. The increased expression of *FGF2* and *FGF18* and reduced expression of *FGF10* suggest a chondroprotective effect based on the reported biological effects of FGF18 [71,72]. The PPI network of this cell senescence-related gene cluster suggested *IL6* and *FGF2* as the core genes interacting with most of the other genes (Fig. 4f). These results provide a framework of the cellular mechanism underlying how tensile loading stimulus regulates stem cell self-renewal, differentiation, and cell senescence related activities.

3.5. Intermittent cyclic tensile loading enhanced ECM production and deposition

The deposition of meniscus-specific ECM components, such as GAGs, by hMeSPCs in 3D hydrogel cultures was significantly increased upon biomimetic loading (Fig. 5a). Safranin O staining showed increased GAGs accumulation in cell-GelMA constructs with increasing culture time, with a significantly higher amount found in loaded groups (Fig. 5a and b). Col I and Col II, representative ECM macromolecules of meniscus tissue [73,74], were also evaluated by immunohistochemistry in these cultures. Col I staining was found mainly surrounding hMeSPCs in

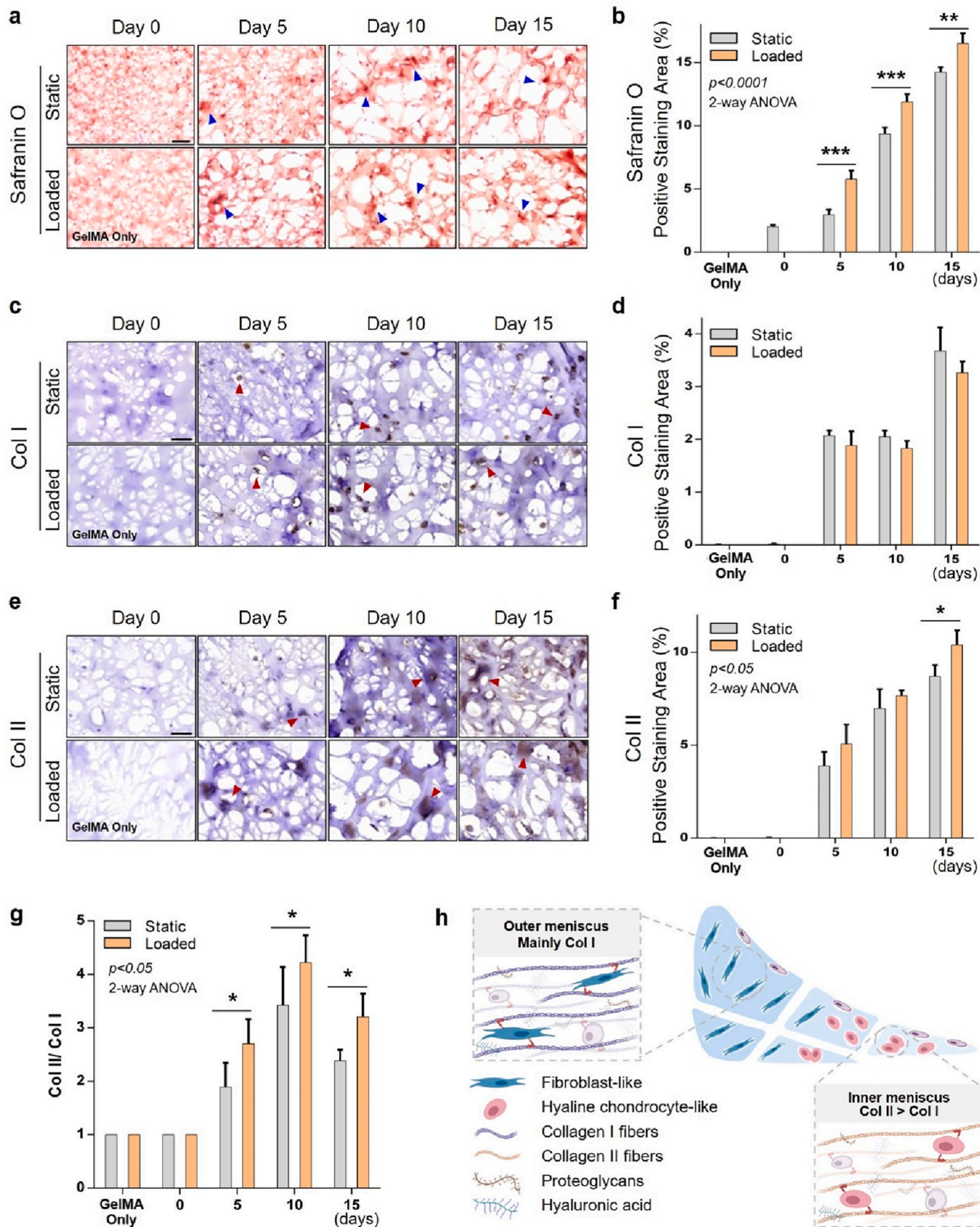
GelMA hydrogel, irrespective of static or loaded culture condition (Fig. 5c). Col I deposition increased with culture time from day 0 to day 15 ($p < 0.05$), but was not significantly different between the static and loaded groups at all time points (Fig. 5d). Meanwhile, Col II deposition also increased with culture time, but was significantly higher in the mechanically stimulated GelMA constructs at day 15 (Fig. 5e and f; day 15, Loaded vs Static, *, $p < 0.05$).

The observation here that mechanical loading promoted ECM deposition in hMeSPCs is consistent with findings from previous reports on other stem/progenitor cell types, including BMSCs [75,76], tendon-derived stem cells [77], and osteoprogenitor and osteoblastic cells [78], suggesting mechanobiological regulation of homeostasis and regeneration in load-bearing tissues. It is noteworthy that intermittent cyclic tensile loading of hMeSPCs resulted in a higher content of Col II relative to Col I in the ECM (Fig. 5g; *, $p < 0.05$ between loaded and static cultures at days 5, 10, and 15), an ECM composition resembling more that of the inner region of native meniscus (Fig. 5h) [79].

In previous studies, our group have investigated the effects of mechanical loading on chondrocytes and MSCs by 2D [80] and 3D cultures [12,81,82], and the enhanced chondrogenic performance was found in both 2D and 3D cultures with proper mechanical stimulation. In current study, from the experiment results at day 15 of loading (in ITS contained, serum free culture condition, no TGF- β was added), we found that the hydrogel encapsulated cells were already differentiated into a chondrogenic like phenotype by mechanical loading, supported by the reduced expression levels of stem cell-like surface markers of CD90, CD73 and CD105 (Fig. 4b) and enhanced cartilage GAG and ECM deposition (Fig. 5). We did not perform chondrogenic differentiation experiments on hydrogel-isolated cells, but we can expect enhanced chondrogenic properties of cells released from the pre-loaded 3D cultures, when they were cultured under standard chondrogenic differentiation protocol, because the standard chondrogenic differentiation protocol is a 3D pellet culture system, with high concentration (10 ng/ml) of TGF- β 1 or TGF- β 3 in the culture medium, which is a more chondrogenic inductive condition compared to cells in hydrogel cultures. Therefore, the current 3D cell-loading culture conditions may have strong potential to enhance the chondrogenic potential of encapsulated stem cells for further application.

It should further be noted that the mechanical stimulations are not the only factor that could regulate the cell behavior. The region-specific ECM components also showed different bioactive effects. In our previous study, we found different bioactive effects on chondrogenic differentiation of hBMSCs by meniscus zonal decellularized ECM (dECM), and have demonstrated that the inner meniscus derived dECM enhances the fibrocartilaginous differentiation of hBMSCs, while the outer meniscus derived dECM promotes a more fibroblastic phenotype [83]. Besides, a recent study by Hee-Woong Yun et al. confirmed that decellularized meniscus ECM has different characteristics according to zone of origin, and expresses zone-specific protein profile (with proteomics and western blot data), and the cells differentiation of synovial mesenchymal stem cells was regulated differently by the zonal specific dECM of meniscus tissue [84]. Moreover, the depth-dependent distribution of matrix contents in the human meniscus may also has mechanical significance in matrix remodeling and cell behavior regulation [85], providing a future direction to explore with more sophisticated methods such as 3D printing with layer-by-layer strategy. Boosting the regenerative capacity of meniscus tissue is a comprehensive task under intensive investigation, and it depends on the cell, ECM, growth factor, and mechanical environment and many other factors.

Nevertheless, research output of current study will empower the further application of tissue resident stem cells in combination with state-of-the-art polymeric scaffolds that possess bioinspired architecture, cell biocompatibility, immune compatibility, growth factor-based bioactivity, and strong mechanical support with advanced manufacturing technologies [86–88], to provide a versatile and promising alternative for the production of advanced zone-specific



(caption on next page)

Fig. 5. Biomimetic tensile loading of hMeSPCs enhanced meniscus-like ECM generation and deposition. (a & b) Safranin O staining of the histologic sections of hMeSPCs-GelMA constructs cultured with (loaded) or without (static) biomimetic loading at 0, 5, 10, and 15 days (a, blue arrowheads indicating positively stained areas), and (b) quantification of Safranin O-stained areas. (c & d) Immunostaining for Col I deposition (c, red arrowheads) in the hMeSPCs-GelMA constructs cultured with or without biomimetic loading at days 0, 5, 10, 15, and (d) quantification of Col I positive staining area. (e) Immunostaining for Col II deposition (e, red arrowheads) by hMeSPCs with or without biomimetic loading at days 0, 5, 10, 15, and (f) quantification of Col II positive staining area. Histological analysis of each hydrogel construct shown above was performed at three different regions of interests (ROIs) of each culture under 10 \times magnification of light microscopy. The positive staining area within GelMA hydrogel structure was quantified using Image J (NIH, US). The experiment was repeated three times with cells from B1, B2 and B3, separately, with 3 technical repeats in each group. Two-way ANOVA with post-hoc between groups; *, $p < 0.05$; **, $p < 0.01$; ***, $p < 0.001$. Data are mean \pm SD, scale bar = 100 μ m. (g) Ratio of Col II to Col I immunostained areas in hMeSPCs-GelMA constructs cultured with (loaded) or without (static) biomimetic loading. Two-way ANOVA with post-hoc between groups; *, $p < 0.05$. Data are mean \pm SD, $n = 3$. (h) Diagrammatic representation of the ECM content in the inner and outer meniscus tissue. **Static, Loaded:** as described in Fig. 3.

fibrocartilaginous tissue and serve as a practical regenerative strategy in future meniscus tissue engineering *in vivo*.

3.6. Cell-hydrogel interaction and ECM dynamic under biomimetic loading

Consistent with previous findings that mechanical loading could accelerate biodegradation of resorbable hydrogel biomaterials [89], we observed faster GelMA degradation upon mechanical loading in both GelMA only and hMeSPC-encapsulated groups, resulting in smaller size, lighter weight, increase in the number and size of pores, i.e., higher porosity, and loss of mechanical strength (Fig. 2g).

The degradation of GelMA hydrogel was firstly observable with Picrosirius Red staining (Fig. 6a, Fig. S4) exhibited as increased number and/or size of pores in histological sections. GelMA degradation was accelerated in response to loading at all times, and was further enhanced by the encapsulation of hMeSPCs, as compared to the GelMA only hydrogel cultures. The histologically observable porosity increased with culture time ($p < 0.0001$) (Fig. 6c). After 15 days of intermittent cyclic tensile loading, higher porosity was seen in both the GelMA only groups ($29.01 \pm 3.37\%$) and GelMA-hMeSPCs groups ($34.81 \pm 0.68\%$), relative to the statically cultured groups ($25.32 \pm 0.75\%$ in GelMA only group; $35.94 \pm 2.88\%$ in GelMA-hMeSPCs group, respectively). In addition, compared with GelMA only groups, hMeSPC encapsulation resulted in a significantly higher porosity in both static cultures, at day 10 (GelMA + cell vs GelMA only, $31.80 \pm 1.47\%$ vs $24.12 \pm 0.36\%$; $p < 0.01$) and day 15 (GelMA + cell vs GelMA only, $35.94 \pm 2.88\%$ vs $25.32 \pm 0.75\%$; $p < 0.001$; and loaded cultures, at day 10 (GelMA + cell vs GelMA only, $34.72 \pm 0.80\%$ vs $28.29 \pm 3.29\%$; $p < 0.05$).

To distinguish between cellular contribution to the nascent ECM deposition and degradation of the GelMA scaffold, a green fluorescence tagged (GFT)-GelMA hydrogel was used to monitor the degradation of GelMA hydrogel with cell encapsulation, under both static and loaded culture regimens. Confocal laser microscopy was used to capture live 3D images. The converted fluorescence intensity heatmap (FIH panels) represents the integrity of GFT-GelMA hydrogel (Fig. 6d), while the daily release of the fluorescent soluble by-products from the GFT-GelMA hydrogel was also profiled (Fig. 6e). As shown in Fig. 6d, increased loss of GFT fluorescence and the corresponding heap map signal clearly showed that both mechanical loading and presence of cells contributed to the faster degradation of GelMA hydrogel scaffold. The progression of hydrogel degradation was further profiled by monitoring the daily release profile of the fluorescent soluble by-products of GFT-GelMA (Fig. 6e). There was a burst of GFT-GelMA release in the first 2 days in all groups, followed by a steady rate of release. The highest levels of GFT-GelMA release were found in the loaded hMeSPC groups, while the GelMA only groups exhibited low release from day 3 to day 15 (Fig. 6e). Interestingly, the results showed that cell encapsulation represented the primary factor in promoting GelMA degradation (e.g., GelMA + cell-Static group vs GelMA only-Static group; *, $p < 0.05$, **, $p < 0.01$, ***, $p < 0.001$; Fig. 6e), whereas mild, biomimetic loading did not significantly accelerate GelMA degradation (e.g., GelMA only-Loaded groups vs GelMA only-Static groups, n.s.; GelMA + cell-Loaded groups vs GelMA + cell-Static groups, n.s.; Fig. 6e).

It is noteworthy that although the presence of encapsulated hMeSPCs resulted in higher scaffold porosity and GelMA release (Fig. 6a–e), with the application of the tensile loading regimen, there no increase in scaffold porosity was observed beyond day 10 (Fig. 6c). Since there was no change in the degradation of GelMA during this period, this observation suggests the possibility that the mechanical loading-associated increase in ECM deposition (see Fig. 5) compensated, at least in part, the degraded GelMA hydrogel.

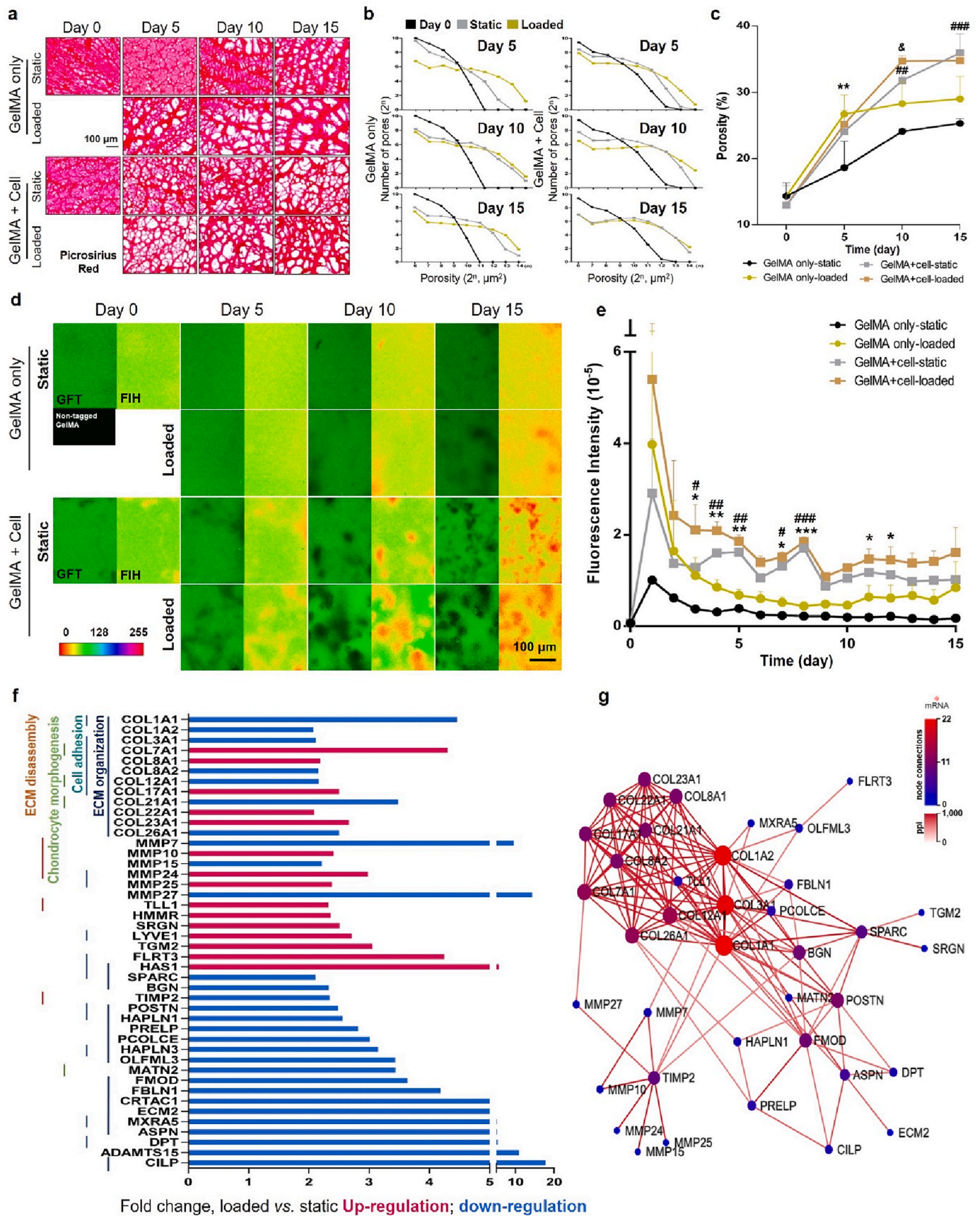
To gain insight into the underlying mechanism of ECM remodeling by the encapsulated cells, another group of mechano-responsive genes were clustered from transcriptomic analysis by virtue of their potential roles in cell-ECM interaction, including cell adhesion, chondrocyte morphogenesis, ECM organization, and ECM disassembly (Fig. 6f). Biomimetic cyclic loading enhanced the expression of *COL7A1*, *COL8A1*, *COL17A1*, *COL22A1* and *COL23A1*, while *COL1A1*, *COL1A2*, *COL3A1*, *COL8A2*, *COL12A1*, *COL21A1* and *COL26A1* were down-regulated, suggesting pericellular matrix re-organization. *COL1A2*, *COL3A1*, *COL1A1* are the core genes in this ECM dynamic gene cluster (Fig. 6g). In addition, biomimetic loading also increased expression of matrix metalloproteinase (MMP) genes, *MMP10*, *MMP24*, *MMP25*, and decreased *MMP7*, *MMP15* and *MMP27* (Fig. 6f), in agreement with previous studies showing that mechanical stress could regulate MMP production [90,91], and suggesting active cell-mediated matrix remodeling in the loaded cultures. On the other hand, the extracellular proteases of the ADAMTS and MMP families that are usually elevated in osteoarthritic chondrocytes, including *ADAMTS2*, *ADAMTS5*, *ADAMTS7*, *ADAMTS14*, *MMP2*, *MMP11*, *MMP13*, and *MMP19* [92], were not significantly altered in this analysis. It is interesting to note that *POSTN*, *COL1A1*, and *TNFSF1*, genes highly expressed in osteoarthritic cartilage [92], were all reduced under intermittent tensile loading (Fig. 6f), suggesting a potential chondroprotective action of mild biomimetic loading.

Other genes expressed differentially with mean absolute fold change of >5 between static and loaded cultures are summarized in Table S3. The mechano-responsive genes were analyzed and grouped into three clusters based on their functions in cell senescence (Fig. 4e and f), mechanical sensitivity (Fig. 3d and e), and ECM dynamics (Fig. 6f and g); these data provide further details for analysis of mechanobiologically regulated cellular activities responsible for ECM dynamic as well as hydrogel scaffold degradation. It should be pointed out that the current study was performed only up to 15 days of culture, and thus limited the investigation to the early phase of the hydrogel degradation (quasi-stable phase and the phase in decrease of strength) [93].

4. Conclusion

With the 3D GelMA hydrogel cyclic loading cell culture system, we found that a “slow walk” biomimetic cyclic loading regimen (10% tensile strain, 0.5 Hz, 1 h/day, up to 15 days) significantly increased (i) hMeSPC differentiation, (ii) fibrocartilage-like ECM deposition, and (iii) the mechanobiological response of 3D encapsulated hMeSPCs and their interactions with GelMA hydrogel.

Mechanophysical influences on cells are known to regulate their differentiation and ECM biosynthesis [75–78]. Recent investigations have shown that cells maintained in more biomimetic 3D cultures



(caption on next page)

Fig. 6. Degradation of GFT-GelMA hydrogel constructs with or without encapsulated hMeSPCs under intermittent tensile loading. (a) Picrosirius Red staining (collagen stain: pink for thin fibers and red for thick fibers) of histologic sections of the hMeSPCs-GelMA constructs under static and loaded conditions at days 0, 5, 10, and 15. Representative micrographs from 3 batches of cultures. Scale bar = 100 μm . (b) Histomorphometric analysis of porosity as a function of culture time, in terms of average pore area (diameter², d^2) and number of pores in the indicated ranges of pore area. (c) Porosity of GelMA constructs with and without encapsulated hMeSPCs cultured under static and loaded conditions at days 0, 5, 10, and 15. Porosity is calculated as total area of pores (number $\times \pi \cdot d^2/4$) expressed as a percentage of total area of the microscopic field. In (b) and (c), data were collected from 3 batches of cultures consisting of cells derived from 9 biological donors, with triplicates as technical repeats. In (c), Two-way ANOVA with post-hoc was used to compare between groups. Data are mean \pm SD. GelMA only-Loaded groups vs GelMA only-Static groups: **, $p < 0.01$; GelMA + cell-Static groups vs GelMA only-Static groups: ##, $p < 0.01$, ###, $p < 0.001$; GelMA + cell-Loaded groups vs GelMA only-Loaded groups: Δ , $p < 0.05$. (d) Representative GFT fluorescence (left panels) and corresponding heatmap intensity of GFT loss (FIH, right panels) images of GFT-GelMA hydrogel constructs with or without encapsulated hMeSPCs cultured under static and loaded conditions at days 0, 5, 10, and 15. Scale bar = 100 μm . Representative micrographs from 3 batches of cultures consisting of cells derived from 9 biological donors. (e) Daily release of fluorescent soluble products derived from degraded GFT-GelMA constructs with or without encapsulated hMeSPCs cultured under static and loaded conditions. GFT-GelMA (60% DS) was used at 10% w/v and hMeSPCs were seeded at 2.5×10^5 cells per 50 μl GelMA. Data (arbitrary units, mean \pm SD) were collected from 3 batches of cultures consisting of cells derived from 9 biological donors, with triplicates as technical repeats. Two-way ANOVA with post-hoc between groups. GelMA + cell-Static groups vs GelMA only-Static groups: *, $p < 0.05$, **, $p < 0.01$, ***, $p < 0.001$; GelMA + cell-Loaded groups vs GelMA only-Loaded groups: #, $p < 0.05$, ##, $p < 0.01$, ###, $p < 0.001$. (f) Expression of ECM dynamic-related genes regulated by intermittent tensile stimulation (loaded vs static; red, up-regulated; blue, down-regulated), and classified by biological function, based on transcriptome analysis described in Fig. 3. (g) Protein-protein interaction network of the corresponding regulated genes. Data were included and analyzed from RNA-seq data intersection of B1 and B2. **Static, Loaded:** as described in Fig. 3.

respond to mechanical cues in a more complex manner than cells in the more conventional 2D monolayer cultures [94]. For the meniscus, with its intrinsic load-bearing function, native tissue homeostasis as well as the maturation of engineered meniscus-like tissues rely critically on the *in vivo* mechanical environment [18,20]. It is recently reported that healthy adult takes approximately 6000–9000 steps/day [95], while advancing age or presence of chronic disease/disability generally reduces levels of activity to 1200–2000 steps/day [96,97]; whether such low activity is sufficient for joint tissue health is currently unknown. The mechanical loading regimen adopted here (10% strain, 0.5 Hz, 1 h/day) was selected to mimic cyclic tensile loading of the meniscus in a "slow walk", in terms of strain, frequency and a low level of daily activity (1800 loads/knee/day, i.e., around 1/2 of average number of steps/day) [95]. The observed effects of this biomimetic mechanical loading on the activities and behavior of hMeSPCs in 3D GelMA hydrogel constructs support the significant contribution of mechanical factors in meniscus tissue maintenance.

This cyclic tensile loading of the 3D hMeSPC constructs, designed to mimic that in the meniscus during slow walk, significantly changed the behavior and activities of the hMeSPCs, in terms of CFU, cell differentiation and fibrocartilage-like ECM deposition. Three hundred and thirty-two mechano-responsive genes were identified. When rendered into cell senescence, mechanical sensitivity, and ECM dynamics associated clusters, different expression levels of interleukins, integrins, and collagens/matrix metalloproteinase pathways are apparent. Specifically, the increased expression levels of integrins (CD49e, CD29) and HA receptor CD44 in hMeSPCs in both mRNA and protein level (Fig. 4b and c) strongly suggest that the cycles of strain and stress relaxation enhance cell-matrix interaction and pericellular matrix reorganization (Figs. 5 and 6d). Moreover, the mechanically loaded hMeSPC groups also exhibited increased fibrocartilage-like ECM accumulation in the GelMA hydrogel (Fig. 5a–g), with a higher ratio of Col II: Col I (Fig. 5g), similar to the ECM of the inner meniscus tissue (Fig. 5h). The stiffness of hydrogel culture substrates likely also contributed to these effects [98], as the mechanical property of GelMA hydrogel in these cultures was similar to that of the inner meniscus ECM (Fig. 1a and b), while after 15 days of loading, the modulus was reduced from 47 kPa to 20 kPa, and the loading-induced decrease in mechanical property to 0.02 MPa resembled that of the PCM of native inner meniscus tissue (Fig. 2g). The decrease in Young's modulus of GelMA-Cell construct after tensile loading is one of many aspects that describing the comprehensive effect of cell-hydrogel cultures, which could be contributed by mechanical stimulation, hydrogel degradation, cell enzymatically digestion, and cell ECM remodeling.

It is noteworthy that, different from previous studies [99], the serum-free, TGF- β -free culture condition used here minimized potential effects of FGF2 and TGF- β s present in serum on stem cell regulation.

To assess how mechanical ECM remodeling, i.e., interplay between matrix degradation and nascent matrix deposition, is affected by mechanical loading, we assembled the hydrogel scaffold with a fluorescently tagged GelMA, GFT-GelMA. This novel approach allowed precise monitoring of matrix degradation, on the basis of both the reduction of fluorescence intensity in the hydrogel biomaterial scaffold and the release of soluble fluorescent degradation product in the medium. Our results showed that while GelMA hydrogel steadily degrades during culture, which was exacerbated by mechanical loading, encapsulated hMeSPCs also actively degraded the GelMA hydrogel. Interestingly, there is some indication that, with extended culture under mechanical loading, the encapsulated hMeSPCs began to contribute to the matrix architecture, as indicated by the lack of increase in porosity of the loaded hMeSPC-GelMA beyond day 10 (Fig. 6a–c). We have summarized these culture time-dependent ECM-associated changes in hMeSPCs in response to biomimetic mechanical loading in Fig. 7. Specifically, the dynamic changes presented are overall hydrogel integrity (red), GelMA degradation (pink), and hMeSPC ECM deposition (green).

In summary, we have developed a novel platform to examine how biomimetic loading regulates a mechano-responsive resident stem/progenitor cell population derived from human meniscus. These *in vitro* findings provide insights on the mechanobiology of meniscal tissue, and strongly suggest that, *in vivo*, a mild activity level similar to that of a slow walk would be beneficial in the maintenance of a cartilage phenotype in the meniscus, in formation that is relevant for the optimization of meniscus tissue engineering and regeneration.

Ethical approval

Human meniscus specimens were obtained from patients undergoing total knee arthroplasty surgeries, with approval from The Chinese University of Hong Kong Clinical Research Ethics Committee (NTEC-CUHK Ref. 2019. 078).

CRediT authorship contribution statement

Jing Sun: Writing – original draft, conceived of the study and drafted the manuscript, designed and performed experiments on actuator establishment, tensile stimulation, and cell biological analysis, contributed equally to this work, performed data collection, performed data interpretation. **Yau Tsz Chan:** performed human meniscus sample collection and cell isolation, performed data collection. **Ki Wai Kevin Ho:** performed human meniscus sample collection and cell isolation, prepared research materials. **Li Zhang:** prepared research materials. **Liming Bian:** performed data collection. **Rocky S. Tuan:** Writing – review & editing, Project administration, edited the manuscript for publication and provided administrative support, performed data

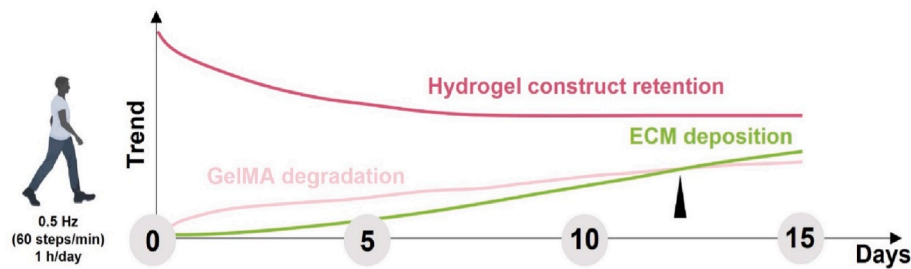


Fig. 7. Diagrammatic representation of ECM dynamics in hMeSPC-GelMA hydrogel constructs cultured under biomimetic tensile loading conditions. Red, hydrogel construct retention; Pink, GelMA degradation; and green, ECM deposition.

interpretation. **Yangzi Jiang:** Supervision, designed, oversaw and supervised the study, Writing – original draft, conceived of the study and drafted the manuscript, designed and performed experiments on actuator establishment, tensile stimulation, and cell biological analysis, contributed equally to this work, prepared research materials, performed data interpretation, Writing – review & editing, Project administration, edited the manuscript for publication and provided administrative support.

Declaration of competing interest

The actuator used for mechanical stimulation in the current study has been applied for patent (US App. No. 63118754; Chinese App. No. 202110356156.3, YJ and JS).

Acknowledgements

This work was supported by the National Key R&D Program [grant number 2019YFA011900, to YJ], administered by the Ministry of Science and Technology of the People's Republic of China (MOST, China); General Research Fund (GRF, grant number 14104022, to YJ) by Hong Kong Research Grants Council, University Grants Committee (RGC, UGC) of Hong Kong SAR, China; The Chinese University of Hong Kong, Impact Postdoctoral Fellowship Scheme [IPDFS, CUHK, to JS]; the Center for Neuromusculoskeletal Restorative Medicine [CNRM at InnoHK, to RST, YJ] by Innovation and Technology Commission (ITC) of Hong Kong SAR, China; and Lee Quo Wei and Lee Yick Hoi Lun Professorship in Tissue Engineering Regenerative Medicine of The Chinese University of Hong Kong (to RST). The authors thank the CORE Facilities of School of Biomedical Sciences, CUHK.

Appendix A. Supplementary data

Supplementary data to this article can be found online at <https://doi.org/10.1016/j.bioactmat.2023.01.025>.

References

- P.S. Walker, M.J. Erkman, The role of the menisci in force transmission across the knee, *Clin. Orthop. Relat. Res.* 109 (1975) 184–192, <https://doi.org/10.1097/00003086-197506000-00027>.
- A.L. McNulty, F. Guilak, Mechanobiology of the meniscus, *J. Biomech.* 48 (8) (2015) 1469–1478, <https://doi.org/10.1016/j.jbiomech.2015.02.008>.
- P.C. Verdonk, et al., Characterisation of human knee meniscus cell phenotype, *Osteoarthritis Cartilage* 13 (7) (2005) 548–560, <https://doi.org/10.1016/j.joca.2005.01.010>.
- H. Sun, et al., Single-cell RNA-seq analysis identifies meniscus progenitors and reveals the progression of meniscus degeneration, *Ann. Rheum. Dis.* 79 (3) (2020) 408–417, <https://doi.org/10.1136/annrheumdis-2019-215926>.
- M. Tissakht, A.M. Ahmed, Tensile stress-strain characteristics of the human meniscal material, *J. Biomech.* 28 (4) (1995) 411–422, [https://doi.org/10.1016/0021-9290\(94\)00081-e](https://doi.org/10.1016/0021-9290(94)00081-e).
- W. Guo, et al., Advances and prospects in tissue-engineered meniscal scaffolds for meniscus regeneration, *Stem Cell. Int.* 2015 (2015), 517520, <https://doi.org/10.1155/2015/517520>.
- H.N. Chia, M.L. Hull, Compressive moduli of the human medial meniscus in the axial and radial directions at equilibrium and at a physiological strain rate, *J. Orthop. Res.* 26 (7) (2008) 951–956, <https://doi.org/10.1002/jor.20573>.
- S.D. McCullen, C.M. Haslauer, E.G. Lobo, Musculoskeletal mechanobiology: interpretation by external force and engineered substratum, *J. Biomech.* 43 (1) (2010) 119–127, <https://doi.org/10.1016/j.jbiomech.2009.09.017>.
- S.E. Szczesny, C.S. Lee, L.J. Soslowsky, Remodeling and repair of orthopedic tissue: role of mechanical loading and biologics, *Am. J. Orthoped.* 39 (11) (2010) 525–530, <http://www.ncbi.nlm.nih.gov/pubmed/21623418>.
- X. Ouyang, Y. Xie, G. Wang, Mechanical stimulation promotes the proliferation and the cartilage phenotype of mesenchymal stem cells and chondrocytes co-cultured in vitro, *Biomed. Pharmacother.* 117 (2019), 109146, <https://doi.org/10.1016/j.biopha.2019.109146>.
- Y. Xie, et al., Proper mechanical stimulation improve the chondrogenic differentiation of mesenchymal stem cells: improve the viscoelasticity and chondrogenic phenotype, *Biomed. Pharmacother.* 115 (2019), 108935, <https://doi.org/10.1016/j.biopha.2019.108935>.
- L. Bian, et al., Dynamic compressive loading enhances cartilage matrix synthesis and distribution and suppresses hypertrophy in hMSC-laden hyaluronic acid hydrogels, *Tissue Eng.* 18 (7–8) (2012) 715–724, <https://doi.org/10.1089/ten.TEA.2011.0455>.
- T.A. Kelly, et al., Spatial and temporal development of chondrocyte-seeded agarose constructs in free-swelling and dynamically loaded cultures, *J. Biomech.* 39 (8) (2006) 1489–1497, <https://doi.org/10.1016/j.jbiomech.2005.03.031>.
- R.L. Mauck, et al., Functional tissue engineering of articular cartilage through dynamic loading of chondrocyte-seeded agarose gels, *J. Biomech. Eng.* 122 (3) (2000) 252–260, <https://doi.org/10.1115/1.429656>.
- J. Sanchez-Adams, R.E. Wilusz, F. Guilak, Atomic force microscopy reveals regional variations in the micromechanical properties of the pericellular and extracellular matrices of the meniscus, *J. Orthop. Res.* 31 (8) (2013) 1218–1225, <https://doi.org/10.1002/jor.22362>.
- T. Kanazawa, et al., Mechanical stretch enhances COL2A1 expression on chromatin by inducing SOX9 nuclear translocation in inner meniscus cells, *J. Orthop. Res.* 30 (3) (2012) 468–474, <https://doi.org/10.1002/jor.21528>.
- B. Fermo, et al., The effects of cyclic mechanical strain and tumor necrosis factor alpha on the response of cells of the meniscus, *Osteoarthritis Cartilage* 12 (12) (2004) 956–962, <https://doi.org/10.1016/j.joca.2004.08.007>.
- B.M. Baker, et al., Dynamic tensile loading improves the functional properties of mesenchymal stem cell-laden nanofiber-based fibrocartilage, *Tissue Eng.* 17 (9–10) (2011) 1445–1455, <https://doi.org/10.1089/ten.TEA.2010.0535>.
- K. Sauerland, J. Steinmeyer, Intermittent mechanical loading of articular cartilage explants modulates chondroitin sulfate fine structure, *Osteoarthritis Cartilage* 15 (12) (2007) 1403–1409, <https://doi.org/10.1016/j.joca.2007.05.004>.
- N.L. Nerurkar, et al., Dynamic culture enhances stem cell infiltration and modulates extracellular matrix production on aligned electrospun nanofibrous scaffolds, *Acta Biomater.* 7 (2) (2011) 485–491, <https://doi.org/10.1016/j.actbio.2010.08.011>.
- J. Gui, J. Zhang, H. Huang, Isolation and characterization of meniscus derived stem cells from rabbit as a possible treatment for damaged meniscus, *Curr. Stem Cell Res. Ther.* 10 (4) (2015) 353–363, <http://www.ncbi.nlm.nih.gov/pubmed/25982534>.
- W. Shen, et al., Intra-articular injection of human meniscus stem/progenitor cells promotes meniscus regeneration and ameliorates osteoarthritis through stromal cell-derived factor-1/CXCR4-mediated homing, *Stem. Cells. Transl. Med.* 3 (3) (2014) 387–394, <https://doi.org/10.5966/sctm.2012-0170>.
- W. Shen, et al., Osteoarthritis prevention through meniscal regeneration induced by intra-articular injection of meniscus stem cells, *Stem Cell. Dev.* 22 (14) (2013) 2071–2082, <https://doi.org/10.1089/scd.2012.0563>.
- S.P. Grogan, et al., Relevance of meniscal cell regional phenotype to tissue engineering, *Connect. Tissue Res.* 58 (3–4) (2017) 259–270, <https://doi.org/10.1080/03008207.2016.1268604>.
- R.L. Mauck, et al., Regional multilineage differentiation potential of meniscal fibrochondrocytes: implications for meniscus repair, *Anat. Rec.* 290 (1) (2007) 48–58, <https://doi.org/10.1002/ar.20419>.
- H. Muhammad, et al., Human migratory meniscus progenitor cells are controlled via the TGF-beta pathway, *Stem Cell Rep.* 3 (5) (2014) 789–803, <https://doi.org/10.1016/j.stemcr.2014.08.010>.

- [27] S.P. Grogan, et al., Digital micromirror device projection printing system for meniscus tissue engineering, *Acta Biomater.* 9 (7) (2013) 7218–7226, <https://doi.org/10.1016/j.actbio.2013.03.020>.
- [28] F. Lin, et al., Injectable hydrogel microspheres in cartilage repair, *Biomed. Technol.* (1) (2023) 18–29, <https://doi.org/10.1016/j.bmt.2022.11.002>.
- [29] Y. Jiang, H. Lin, R.S. Tuan, Overview: state of the art and future perspectives for cartilage repair, in: S. Grässel, A. Aszödi (Eds.), *Cartilage: Volume 3: Repair Strategies and Regeneration*, Springer International Publishing, Cham, 2017, pp. 1–34.
- [30] L. Cai, et al., Microfluidics-derived microcarrier systems for oral delivery, *Biomed. Technol.* (1) (2023) 30–38, <https://doi.org/10.1016/j.bmt.2022.11.001>.
- [31] K.H. Vining, D.J. Mooney, Mechanical forces direct stem cell behaviour in development and regeneration, *Nat. Rev. Mol. Cell Biol.* 18 (12) (2017) 728–742, <https://doi.org/10.1038/nrm.2017.108>.
- [32] S.K. Seidlits, et al., Peptide-modified, hyaluronic acid-based hydrogels as a 3D culture platform for neural stem/progenitor cell engineering, *J. Biomed. Mater. Res. A.* 107 (4) (2019) 704–718, <https://doi.org/10.1002/jbm.a.36603>.
- [33] A.M. Greiner, et al., Cell type-specific adaptation of cellular and nuclear volume in micro-engineered 3D environments, *Biomaterials* 69 (2015) 121–132, <https://doi.org/10.1016/j.biomaterials.2015.08.016>.
- [34] B.L. Ekerdt, et al., Thermoreversible hyaluronic acid-PNIPAAm hydrogel systems for 3D stem cell culture, *Adv. Healthc. Mater.* 7 (12) (2018), e1800225, <https://doi.org/10.1002/adhm.201800225>.
- [35] J. Lou, et al., Stress relaxing hyaluronic acid-collagen hydrogels promote cell spreading, fiber remodeling, and focal adhesion formation in 3D cell culture, *Biomaterials* 154 (2018) 213–222, <https://doi.org/10.1016/j.biomaterials.2017.11.004>.
- [36] S.P. Grogan, et al., Gene expression profiles of the meniscus avascular phenotype: a guide for meniscus tissue engineering, *J. Orthop. Res.* 36 (7) (2018) 1947–1958, <https://doi.org/10.1002/jor.23864>.
- [37] W. Schuurman, et al., Gelatin-methacrylamide hydrogels as potential biomaterials for fabrication of tissue-engineered cartilage constructs, *Macromol. Biosci.* 13 (5) (2013) 551–561, <https://doi.org/10.1002/mabi.201200471>.
- [38] K. Yue, et al., Synthesis, properties, and biomedical applications of gelatin methacryloyl (GelMA) hydrogels, *Biomaterials* 73 (2015) 254–271, <https://doi.org/10.1016/j.biomaterials.2015.08.045>.
- [39] C. Liu, et al., Influence of perfusion and compression on the proliferation and differentiation of bone mesenchymal stromal cells seeded on polyurethane scaffolds, *Biomaterials* 33 (4) (2012) 1052–1064, <https://doi.org/10.1016/j.biomaterials.2011.10.041>.
- [40] M. Petri, et al., Effects of perfusion and cyclic compression on in vitro tissue engineered meniscus implants, *Knee Surg. Sports Traumatol. Arthrosc.* 20 (2) (2012) 223–231, <https://doi.org/10.1007/s00167-011-1600-3>.
- [41] D.W. Youngstrom, et al., A bioreactor system for in vitro tendon differentiation and tendon tissue engineering, *J. Orthop. Res.* 33 (6) (2015) 911–918, <https://doi.org/10.1002/jor.22848>.
- [42] T. Wang, et al., Programmable mechanical stimulation influences tendon homeostasis in a bioreactor system, *Biotechnol. Bioeng.* 110 (5) (2013) 1495–1507, <https://doi.org/10.1002/bit.24809>.
- [43] L.A. Bosworth, et al., Dynamic loading of electrospun yarns guides mesenchymal stem cells towards a tendon lineage, *J. Mech. Behav. Biomed. Mater.* 39 (2014) 175–183, <https://doi.org/10.1016/j.jmbmb.2014.07.009>.
- [44] H. Lin, et al., Cartilage tissue engineering application of injectable gelatin hydrogel with in situ visible-light-activated gelation capability in both air and aqueous solution, *Tissue Eng.* 20 (17–18) (2014) 2402–2411, <https://doi.org/10.1089/ten.TEA.2013.0642>.
- [45] C. Kilic Bektas, V. Hasirci, Cell loaded 3D bioprinted GelMA hydrogels for corneal stroma engineering, *Biomater. Sci.* 8 (1) (2019) 438–449, <https://doi.org/10.1039/c9bm01236b>.
- [46] M.P. Heliö Le Graverand, et al., The cells of the rabbit meniscus: their arrangement, interrelationship, morphological variations and cytoarchitecture, *J. Anat.* 198 (Pt 5) (2001) 525–535, <https://doi.org/10.1046/j.1469-7580.2000.19850525.x>.
- [47] K. Nakata, et al., Human meniscus cell: characterization of the primary culture and use for tissue engineering, *Clin. Orthop. Relat. Res.* (391 Suppl) (2001) S208–S218, <http://www.ncbi.nlm.nih.gov/pubmed/11603705>.
- [48] F. Halbwirth, et al., Mechanostimulation changes the catabolic phenotype of human dedifferentiated osteoarthritic chondrocytes, *Knee Surg. Sports Traumatol. Arthrosc.* 23 (1) (2015) 104–111, <https://doi.org/10.1007/s00167-014-3412-8>.
- [49] Y. Wang, et al., Effect of alginate culture and mechanical stimulation on cartilaginous matrix synthesis of rat dedifferentiated chondrocytes, *Bio Med. Mater. Eng.* 18 (1 Suppl) (2008) S47–S54, <http://www.ncbi.nlm.nih.gov/pubmed/18334723>.
- [50] K. Chokalingam, et al., Three-dimensional in vitro effects of compression and time in culture on aggregate modulus and on gene expression and protein content of collagen type II in murine chondrocytes, *Tissue Eng.* 15 (10) (2009) 2807–2816, <https://doi.org/10.1089/ten.TEA.2008.0560>.
- [51] P. Singh, J.E. Schwarzbauer, Fibronectin and stem cell differentiation - lessons from chondrogenesis, *J. Cell Sci.* 125 (16) (2012) 3703–3712, <https://doi.org/10.1242/jcs.095786>.
- [52] J.I. Pulai, M. Del Carlo Jr., R.F. Loeser, The alpha5beta1 integrin provides matrix survival signals for normal and osteoarthritic human articular chondrocytes in vitro, *Arthritis Rheum.* 46 (6) (2002) 1528–1535, <https://doi.org/10.1002/art.10334>.
- [53] U. Kachroo, B. Ramasamy, E. Vinod, Evaluation of CD49e as a distinguishing marker for human articular cartilage derived chondroprogenitors, *Knee* 27 (3) (2020) 833–837, <https://doi.org/10.1016/j.knee.2020.04.002>.
- [54] E. Vinod, et al., Comparative analysis of fresh chondrocytes, cultured chondrocytes and chondroprogenitors derived from human articular cartilage, *Acta Histochem.* 122 (1) (2020), 151462, <https://doi.org/10.1016/j.acthis.2019.151462>.
- [55] S. Yin, et al., Chondrogenic transdifferentiation of human dermal fibroblasts stimulated with cartilage-derived morphogenetic protein 1, *Tissue Eng.* 16 (5) (2010) 1633–1643, <https://doi.org/10.1089/ten.TEA.2009.0570>.
- [56] E. Lucchinetti, M.M. Bhargava, P.A. Torzilli, The effect of mechanical load on integrin subunits alpha5 and beta1 in chondrocytes from mature and immature cartilage explants, *Cell Tissue Res.* 315 (3) (2004) 385–391, <https://doi.org/10.1007/s00441-003-0836-8>.
- [57] R.F. Loeser, Integrins and chondrocyte-matrix interactions in articular cartilage, *Matrix Biol.* 39 (2014) 11–16, <https://doi.org/10.1016/j.matbio.2014.08.007>.
- [58] N. Sassi, et al., The roles of canonical and non-canonical Wnt signaling in human de-differentiated articular chondrocytes, *Biotech. Histochem.* 89 (1) (2014) 53–65, <https://doi.org/10.3109/10520295.2013.819123>.
- [59] K. Kumawat, R. Gosens, WNT-5A: signaling and functions in health and disease, *Cell. Mol. Life Sci.* 73 (3) (2016) 567–587, <https://doi.org/10.1007/s00018-015-2076-y>.
- [60] G. Nalesso, et al., WNT-3A modulates articular chondrocyte phenotype by activating both canonical and noncanonical pathways, *J. Cell Biol.* 193 (3) (2011) 551–564, <https://doi.org/10.1083/jcb.201011051>.
- [61] R.S. Thomas, et al., Effects of Wnt3A and mechanical load on cartilage chondrocyte homeostasis, *Arthritis Res. Ther.* 13 (6) (2011) R203, <https://doi.org/10.1186/ar3536>.
- [62] J. Elayyan, et al., LEF1-mediated MMP13 gene expression is repressed by SIRT1 in human chondrocytes, *Faseb. J.* 31 (7) (2017) 3116–3125, <https://doi.org/10.1096/fj.201601253R>.
- [63] R.A. Rolfe, et al., Identification of mechanosensitive genes during skeletal development: alteration of genes associated with cytoskeletal rearrangement and cell signalling pathways, *BMC Genom.* 15 (2014) 48, <https://doi.org/10.1186/1471-2164-15-48>.
- [64] B.A. Kerr, et al., Kindlin-3 mutation in mesenchymal stem cells results in enhanced chondrogenesis, *Exp. Cell Res.* 399 (2) (2021), 112456, <https://doi.org/10.1016/j.yexcr.2020.112456>.
- [65] H. Wang, et al., R-Spondin 1 promotes vibration-induced bone formation in mouse models of osteoporosis, *J. Mol. Med.* 91 (12) (2013) 1421–1429, <https://doi.org/10.1007/s00109-013-1068-3>.
- [66] Y.H. Lee, et al., Differential expression patterns of rpondin family and leucine-rich repeat-containing G-protein coupled receptors in chondrocytes and osteoblasts, *Cell J.* 22 (4) (2021) 437–449, <https://doi.org/10.22074/cellj.2021.6927>.
- [67] S. Brielle, et al., Delineating the heterogeneity of matrix-directed differentiation toward soft and stiff tissue lineages via single-cell profiling, *Proc. Natl. Acad. Sci. USA* 118 (19) (2021), <https://doi.org/10.1073/pnas.2016322118>.
- [68] A. Wiesmann, et al., Decreased CD90 expression in human mesenchymal stem cells by applying mechanical stimulation, *Head Face Med.* 2 (2006) 8, <https://doi.org/10.1186/1746-160X-2-8>.
- [69] S.C. Wu, et al., Hyaluronan initiates chondrogenesis mainly via CD44 in human adipose-derived stem cells, *J. Appl. Physiol.* 114 (11) (2013) 1610–1618, <https://doi.org/10.1152/jappphysiol.01132.2012>.
- [70] F. Meng, et al., Hyaluronan size alters chondrogenesis of mesenchymal stem cells cultured on tricalcium phosphate-collagen-hyaluronan scaffolds, *J. Biomed. Mater. Res.* 110 (4) (2022) 838–850, <https://doi.org/10.1002/jbm.a.37332>.
- [71] J.L. Ellsworth, et al., Fibroblast growth factor-18 is a trophic factor for mature chondrocytes and their progenitors, *Osteoarthritis Cartilage* 10 (4) (2002) 308–320, <https://doi.org/10.1053/joca.2002.0514>.
- [72] E.E. Moore, et al., Fibroblast growth factor-18 stimulates chondrogenesis and cartilage repair in a rat model of injury-induced osteoarthritis, *Osteoarthritis Cartilage* 13 (7) (2005) 623–631, <https://doi.org/10.1016/j.joca.2005.03.003>.
- [73] D.C. Fithian, M.A. Kelly, V.C. Mow, Material properties and structure-function relationships in the menisci, *Clin. Orthop. Relat. Res.* (252) (1990) 19–31, <http://www.ncbi.nlm.nih.gov/pubmed/2406069>.
- [74] E.A. Makris, P. Hadidi, K.A. Athanasiou, The knee meniscus: structure-function, pathophysiology, current repair techniques, and prospects for regeneration, *Biomaterials* 32 (30) (2011) 7411–7431, <https://doi.org/10.1016/j.biomaterials.2011.06.037>.
- [75] B. Engebretson, Z.R. Mussett, V.I. Sikavitsas, Tenocytic extract and mechanical stimulation in a tissue-engineered tendon construct increases cellular proliferation and ECM deposition, *Biotechnol. J.* 12 (3) (2017), <https://doi.org/10.1002/biot.201600595>.
- [76] C.K. Kuo, R.S. Tuan, Mechanoactive tenogenic differentiation of human mesenchymal stem cells, *Tissue Eng.* 14 (10) (2008) 1615–1627, <https://doi.org/10.1089/ten.tea.2006.0415>.
- [77] Y. Xu, et al., Cyclic tensile strain induces tenogenic differentiation of tendon-derived stem cells in bioreactor culture, *BioMed Res. Int.* 2015 (2015), 790804, <https://doi.org/10.1155/2015/790804>.
- [78] Y. Guo, et al., Mechanical strain promotes osteoblast ECM formation and improves its osteoinductive potential, *Biomed. Eng. Online* 11 (2012) 80, <https://doi.org/10.1186/1475-925X-11-80>.
- [79] M.L. Upton, J. Chen, L.A. Setton, Region-specific constitutive gene expression in the adult porcine meniscus, *J. Orthop. Res.* 24 (7) (2006) 1562–1570.
- [80] X. Xie, et al., Platelet-rich plasma inhibits mechanically induced injury in chondrocytes, *Arthroscopy* 31 (6) (2015) 1142–1150, <https://doi.org/10.1016/j.arthro.2015.01.007>.

- [81] R.L. Mauck, et al., Regulation of cartilaginous ECM gene transcription by chondrocytes and MSCs in 3D culture in response to dynamic loading, *Biomech. Model. Mechanobiol.* 6 (1–2) (2007) 113–125, <https://doi.org/10.1007/s10237-006-0042-1>.
- [82] E.G. Lima, et al., The beneficial effect of delayed compressive loading on tissue-engineered cartilage constructs cultured with TGF-beta3, *Osteoarthritis Cartilage* 15 (9) (2007) 1025–1033, <https://doi.org/10.1016/j.joca.2007.03.008>.
- [83] K. Shimomura, B.B. Rothrauff, R.S. Tuan, Region-specific effect of the decellularized meniscus extracellular matrix on mesenchymal stem cell-based meniscus tissue engineering, *Am. J. Sports Med.* 45 (3) (2017) 604–611, <https://doi.org/10.1177/0363546516674184>.
- [84] H.W. Yun, et al., Fabrication of decellularized meniscus extracellular matrix according to inner cartilaginous, middle transitional, and outer fibrous zones result in zone-specific protein expression useful for precise replication of meniscus zones, *Mater. Sci. Eng. C. Mater. Biol. Appl.* 128 (2021), 112312, <https://doi.org/10.1016/j.msec.2021.112312>.
- [85] J.M. Parraga Quiroga, et al., Should a native depth-dependent distribution of human meniscus constitutive components be considered in FEA-models of the knee joint? *J. Mech. Behav. Biomed. Mater.* 38 (2014) 242–250, <https://doi.org/10.1016/j.jmbbm.2014.03.005>.
- [86] S. Chae, et al., 3D cell-printing of biocompatible and functional meniscus constructs using meniscus-derived bioink, *Biomaterials* 267 (2021), 120466, <https://doi.org/10.1016/j.biomaterials.2020.120466>.
- [87] H. Li, et al., Meniscal regenerative scaffolds based on biopolymers and polymers: recent status and applications, *Front. Cell Dev. Biol.* 9 (2021), 661802, <https://doi.org/10.3389/fcell.2021.661802>.
- [88] Z.Z. Zhang, et al., Orchestrated biomechanical, structural, and biochemical stimuli for engineering anisotropic meniscus, *Sci. Transl. Med.* 11 (487) (2019), <https://doi.org/10.1126/scitranslmed.aao0750>.
- [89] E. Piskin, et al., In vivo performance of simvastatin-loaded electrospun spiral-wound polycaprolactone scaffolds in reconstruction of cranial bone defects in the rat model, *J. Biomed. Mater. Res. A.* 90 (4) (2009) 1137–1151, <https://doi.org/10.1002/jbm.a.32157>.
- [90] J.D. Kisiday, et al., Evaluation of adult equine bone marrow- and adipose-derived progenitor cell chondrogenesis in hydrogel cultures, *J. Orthop. Res.* 26 (3) (2008) 322–331, <https://doi.org/10.1002/jor.20508>.
- [91] S.J. Kim, et al., Therapeutic effects of neuropeptide substance P coupled with self-assembled peptide nanofibers on the progression of osteoarthritis in a rat model, *Biomaterials* 74 (2016) 119–130, <https://doi.org/10.1016/j.biomaterials.2015.09.040>.
- [92] K.M. Fisch, et al., Identification of transcription factors responsible for dysregulated networks in human osteoarthritis cartilage by global gene expression analysis, *Osteoarthritis Cartilage* 26 (11) (2018) 1531–1538, <https://doi.org/10.1016/j.joca.2018.07.012>.
- [93] N. Bolgen, et al., In vitro and in vivo degradation of non-woven materials made of poly(epsilon-caprolactone) nanofibers prepared by electrospinning under different conditions, *J. Biomater. Sci. Polym. Ed.* 16 (12) (2005) 1537–1555, <https://doi.org/10.1163/156856205774576655>.
- [94] S.R. Rathbone, et al., Cyclic tensile strain upon human mesenchymal stem cells in 2D and 3D culture differentially influences CCN2, WDR61 and BAHCC1 gene expression levels, *J. Mech. Behav. Biomed. Mater.* 11 (2012) 82–91, <https://doi.org/10.1016/j.jmbbm.2012.01.019>.
- [95] T. Althoff, et al., Large-scale physical activity data reveal worldwide activity inequality, *Nature* 547 (7663) (2017) 336–339, <https://doi.org/10.1038/nature23018>.
- [96] C. Tudor-Locke, T.L. Washington, T.L. Hart, Expected values for steps/day in special populations, *Prev. Med.* 49 (1) (2009) 3–11, <https://doi.org/10.1016/j.ypmed.2009.04.012>.
- [97] C. Tudor-Locke, et al., How many steps/day are enough? For older adults and special populations, *Int. J. Behav. Nutr. Phys. Activ.* 8 (2011) 80, <https://doi.org/10.1186/1479-5868-8-80>.
- [98] A.J. Engler, et al., Matrix elasticity directs stem cell lineage specification, *Cell* 126 (4) (2006) 677–689, <https://doi.org/10.1016/j.cell.2006.06.044>.
- [99] S.F. Carroll, C.T. Buckley, D.J. Kelly, Cyclic tensile strain can play a role in directing both intramembranous and endochondral ossification of mesenchymal stem cells, *Front. Bioeng. Biotechnol.* 5 (2017) 73, <https://doi.org/10.3389/fbioe.2017.00073>.